Human Molecular Genetics, 2018, Vol. 27, No. 23 4117–4134

doi: 10.1093/hmg/ddy304
Advance Access Publication Date: 24 August 2018
General Article

GENERAL ARTICLE

Mechanism suppressing H3K9 trimethylation in pluripotent stem cells and its demise by polyQ-expanded huntingtin mutations

Dilber Irmak[1,#], Azra Fatima[1,#], Ricardo Gutiérrez-Garcia[1], Markus M. Rinschen[1], Prerana Wagle[1], Janine Altmüller[2,3], Laura Arrigoni[4], Barbara Hummel[4], Corinna Klein[1], Christian K. Frese[1], Ritwick Sawarkar[4], Alvaro Rada-Iglesias[1,2] and David Vilchez[1,*,†]

[1]Cologne Excellence Cluster for Cellular Stress Responses in Aging-Associated Diseases (CECAD), University of Cologne, Joseph-Stelzmann-Strasse 26, Cologne 50931, Germany, [2]Center for Molecular Medicine Cologne (CMMC), University of Cologne, Robert-Koch-Strasse 21, Cologne 50931, Germany, [3]Cologne Center for Genomics (CCG), University of Cologne, Cologne 50931, Germany and [4]Max Planck Institute of Immunobiology and Epigenetics, Freiburg 79108, Germany

*To whom correspondence should be addressed at: Cologne Excellence Cluster for Cellular Stress Responses in Aging-Associated Diseases (CECAD), University of Cologne, Joseph-Stelzmann-Strasse 26, Cologne 50931, Germany. Tel: +49 22147884172; Fax: +49 221 478 84045; Email: dvilchez@uni-koeln.de

Abstract

Pluripotent stem cells are invaluable resources to study development and disease, holding a great promise for regenerative medicine. Here we use human embryonic stem cells (hESCs) and induced pluripotent stem cells (iPSCs) from patients with Huntington's disease (HD-iPSCs) to shed light into the normal function of huntingtin (HTT) and its demise in disease. We find that HTT binds ATF7IP, a regulator of the histone H3 methyltransferase SETDB1. HTT inhibits the interaction of the ATF7IP-SETDB1 complex with other heterochromatin regulators and transcriptional repressors, maintaining low levels of H3K9 trimethylation (H3K9me3) in hESCs. Loss of HTT promotes global increased H3K9me3 levels and enrichment of H3K9me3 marks at distinct genes, including transcriptional regulators of neuronal differentiation. Although these genes are normally expressed at low amounts in hESCs, HTT knockdown (KD) reduces their induction during neural differentiation. Notably, mutant expanded polyglutamine repeats in HTT diminish its interaction with ATF7IP-SETDB1 complex and trigger H3K9me3 in HD-iPSCs. Conversely, KD of ATF7IP in HD-iPSCs reduces H3K9me3 alterations and ameliorates gene expression changes in their neural counterparts. Taken together, our results indicate ATF7IP as a potential target to correct aberrant H3K9me3 levels induced by mutant HTT.

†David Vilchez, http://orcid.org/0000-0002-0801-0743
#These authors contributed equally.

Received: May 9, 2018. **Revised:** August 9, 2018. **Accepted:** August 10, 2018

Introduction

Huntington's disease (HD) is an autosomal dominant neurodegenerative disorder caused by mutations in the *huntingtin* (*HTT*) gene (1,2). These mutations expand the CAG triplet repeat region in exon 1, resulting in an unstable polyglutamine (polyQ) stretch in the protein. In its wild-type form, HTT contains 6–35 glutamine residues. However, in individuals affected by HD, it contains greater than 35 polyQ repeats. Although HTT is ubiquitously expressed (3,4), mutant HTT particularly leads to neuronal dysfunction and death in many brain regions with the striatum undergoing the greatest neurodegeneration (5). Extensive data and the dominant inheritance pattern of HD indicate that gain-of-function of mutant HTT is toxic and triggers neurodegeneration (1). However, growing evidence suggests that loss of normal HTT function also contributes to HD (3,4). For instance, down-regulation of wild-type HTT levels induces HD-related changes such as progressive neurodegeneration and motor dysfunction or hastens these changes in HD models (6–10). Moreover, ectopic expression of wild-type HTT improves brain cell survival and ameliorates the deleterious effects of the mutant protein (7,11–17).

Remarkably, conditional knockout of *Htt* in mice at embryonic day 14.5 causes progressive neurodegeneration that mimics HD phenotypes (6). At earlier stages, complete depletion of HTT results in severe neural developmental defects and embryonic lethality (18–20), providing a link between normal function of HTT and development. Mice with reduced levels of HTT to below 50% bypass the lethality phenotype but display aberrant brain development, suggesting a role of HTT in neurogenesis (21). Loss of HTT during embryonic neurogenesis decreases the pool of cortical progenitors by accelerating their differentiation, a process that results in altered cell fate decisions (22). *In vitro*, neural progenitor cells (NPCs) derived from $Htt^{-/-}$ mouse embryonic stem cells (mESCs) can be terminally differentiated into neurons. However, a study demonstrated that their neuronal differentiation efficiency is altered as they tend to give rise to more astrocytes compared with wild-type NPCs (23). Another study finds even earlier phenotypes such as decreased self-renewal, increased cell death and alterations in the lineage potential of NPCs derived from $Htt^{-/-}$ mESCs (24). Although HD patients and mouse models do not exhibit striking developmental phenotypes as HTT knockout models (3,21,25,26), cumulative evidence indicates developmental deficits in HD mouse models and human pathological specimens (27–30). For instance, polyQ-expanded HTT induces deficits such as impairment in the maintenance of striatal neural stem cells and their specification into medium spiny neurons (30). Furthermore, both HD patients and mouse models present abnormalities in brain morphology and synaptic plasticity before the onset of apparent clinical deficits (31–37). When mESCs are genetically modified to express polyQ-expanded HTT, they maintain their ability to generate NPCs. Upon neuronal induction, these cells exhibit a higher percentage of neuronal death resulting in reduced number of neurons remaining at the end of the differentiation process (23). Likewise, HD-iPSCs from the patients differentiate into NPCs with indistinguishable efficiency, although these progenitors manifest abnormalities in cytoskeleton, cell adhesion, energetics and expression of neural developmental factors (38). Nevertheless, HD-NPCs can be terminally differentiated into neurons with alterations in calcium homeostasis and electrophysiology, increased vulnerability to excitotoxic stressors as well as cumulative risk of death over time (38). Moreover, neural cultures differentiated from HD-iPSCs containing neurons, astrocytes and NPCs present HD-related transcriptional changes consistent with those observed in the HD brain, including neurodevelopmental transcription factors and genes involved in axonal guidance, calcium influx or gamma-Aminobutyric acid (GABA) signaling (e.g. GABA receptors) (39). In fact, transcriptional dysregulation is a prominent defect observed in postmortem HD brains and distinct HD mouse models [reviewed in (4,40)]. An increasing number of studies provide evidence of alterations in epigenetic marks such as DNA methylation and post-translational modifications of histone proteins (e.g. H3K3me3) that can contribute to aberrant gene expression in HD patients as well as HD cellular and organismal models (40–48). In these lines, neural cultures differentiated from HD-iPSCs exhibit H3K4me3 and H3K27ac epigenetic alterations (39). Likewise, targeted mutations that expand the CAG stretch in one HTT allele are sufficient to impair H3K4me3 marks in both mESCs and their NPC counterparts (49). A direct role of HTT in these phenotypes is supported by nuclear export (NES) and nuclear localization signals within the protein, allowing for its nuclear localization (50). In addition, polyQ-expanded mutations impair nuclear export of HTT (51).

Thus, HTT-mediated epigenetic alterations could contribute to transcriptional abnormalities in HD (44). Among these epigenetic changes, H3K9 trimethylation (H3K9me3) is robustly increased in HD patients and HD mouse models (52–55). H3K9 hypermethylation is accompanied by up-regulation of its specific methyltransferase SETDB1 (54). H3K9me3 is associated with heterochromatin and correlates with transcriptional repression (56). In human pluripotent stem cells, the levels of heterochromatin-associated histone modifications such as H3K9me3 are usually reduced whereas the levels of transcriptional activations marks such as acetylated histones are generally increased (57,58). These observations raise an intriguing question: does HTT maintain low H3K9me3 levels in pluripotent stem cells?

Here we show that HTT interacts with ATF7IP, a chromatin factor that regulates SETDB1 activity at heterochromatin formation sites to facilitate trimethylation of H3K9 (59,60). Knockdown (KD) of HTT alters the nuclear location of ATF7IP and promotes its interaction with heterochromatin regulators and transcriptional repressors, resulting in higher global H3K9me3. Thus, HTT maintains the H3K9me3 landscape of human embryonic stem cells (hESCs). Conversely, loss of HTT results in enrichment of H3K9me3 marks in multiple genes, including transcriptional regulators of neuronal differentiation (e.g. ASCL2, GBX1). Moreover, H3K9me3 repressive marks at the pluripotent stem cell stage correlate with reduced induction of these genes during neural differentiation. We find that expanded polyQ diminishes the interaction of mutant HTT with ATF7IP and triggers H3K9me3 in HD-iPSCs. Notably, KD of ATF7IP decreases H3K9me3 levels in HD-iPSCs. Taken together, our results indicate a direct role of HTT in the regulation of H3K9me3 via its interaction with the ATF7IP-SETDB1 complex, providing a target to correct H3K9me3 changes induced by polyQ-expanded HTT.

Results

HTT interacts with the chromatin regulator ATF7IP

We found that hESCs exhibit higher expression of HTT than their differentiated neuronal counterparts at both protein and messenger RNA (mRNA) levels (Fig. 1A and B), supporting a role of HTT in hESC identity. To determine the protein binding

Table 1. Protein interactors of HTT in H9 hESCs

Protein names	T-test difference	-log P-value
HTT	9.96	1.25
F8A1	7.69	1.33
NUP205	7.00	2.23
ASPSCR1	5.61	4.17
ATF7IP	5.55	1.08
VCP	5.30	2.01
U2AF2	1.76	3.42

Protein LFQ values from co-IP experiments using HTT antibody compared to control co-IP with FLAG antibody (FDR < 0.05 was considered significant).

partners of HTT in hESCs, we performed co-immunoprecipitation (co-IP) experiments followed by a single shot label-free proteomic approach. We quantified ~2000 proteins and compared protein abundance in HTT antibody pulldowns with control FLAG antibody pulldowns in both hESCs and terminally differentiated neurons (Supplementary Data 1). Although HTT was the most enriched protein in both hESCs and neurons (Fig. 1C and D and Supplementary Data 1), hierarchical clustering revealed a clear separation in HTT-interacting proteins between these cells (Supplementary Material, Fig. S1). Consistent with increased HTT expression in hESCs (Fig. 1A), we obtained higher amounts of immunoprecipitated HTT in these cells when compared to neurons (9.96 versus 6.57 $\log_2$-fold enrichment, respectively) (Fig. 1E and Supplementary Data 1). On the contrary, a major population of proteins specifically interacted with HTT in neurons, but not in hESCs (Fig. 1E and F and Supplementary Data 1). Whereas 102 proteins passed the criterions for significant interaction with HTT in neurons (Fig. 1D), only seven proteins were significantly detected in hESCs (Fig. 1C and Table 1). Among them, NUP201 and U2AF2 were exclusively co-immunoprecipitated in hESCs whereas the other five proteins were also detected in neurons (Fig. 1F), including HTT itself and its known interactors F8A1 (61) and VCP (62). In both hESCs and neurons, we found a novel interaction of HTT with ATF7IP (Fig. 1C and D). This transcriptional repressor forms a complex with the H3K9 methyltransferase SETDB1, which can translocate to DNA-methylated sites inducing H3K9me3 and concomitant heterochromatin formation (59,60,63–65). Notably, co-IP experiments followed by western blot indicated that HTT could form a complex with both ATF7IP and SETDB1 (Fig. 1G). Thus, our results suggest that HTT interacts with key epigenetic regulators.

Loss of HTT alters ATF7IP interactions and induces H3K9me3 in hESCs

The interaction of ATF7IP-SETDB1 with MBD1, a protein that binds methylated DNA, results in catalytic activation of SETDB1 and H3K9me3 (59,60,63,64). Moreover, ATF7IP stabilizes SETDB1 in the nucleus of human cell lines (65). We found that the KD of ATF7IP dramatically diminishes nuclear SETDB1 levels as well as trimethylation of H3K9 in hESCs (Fig. 2A and B), indicating that ATF7IP also regulates H3K9me3 in these cells. Interestingly, reduction of H3K9me3 upon loss of ATF7IP did not affect the expression of pluripotency markers as assessed by quantitative polymerase chain reaction (qPCR) (Fig. 2C). To further examine changes induced by loss of ATF7IP in hESCs, we performed transcriptomic analysis (Supplementary Data 2). These experiments revealed significant changes [fold change (FC) > 2, P-value < 0.05] in the steady-state levels of 565 transcripts. Among them, 475 transcripts were up-regulated, of which gene ontology biological processes (GOBPs) term analysis indicated a strong enrichment for modulators of transcription, nervous system development, neuronal differentiation, axon guidance and WNT signaling, a regulatory node of neural differentiation (66) (Supplementary Material, Fig. S2 and Supplementary Data 2).

Given that HTT interacted with ATF7IP (Fig. 1), we assessed whether modulation of HTT impairs H3K9me3 in hESCs, which normally have low H3K9me3 levels when compared to differentiated cells (57,58). Indeed, we observed a dramatic increase in H3K9me3 levels upon HTT KD (Fig. 2D and E). Since hESCs can vary in their characteristics, we examined an independent hESC line and obtained similar results (Supplementary Material, Fig. S3A and B). With the role of HTT in brain development (21), we asked whether alterations in H3K9me3 levels of hESCs are transmitted to their NPC counterparts. For this purpose, we performed neural induction of HTT KD hESCs. After 10 days of neural induction, the expression of the early neuroectodermal marker PAX6 (67) as well as other neural markers were triggered at the same extent in both control and HTT KD cells (Supplementary Material, Fig. S4A–C). These results indicate that HTT is not required for hESC commitment into NPCs. To further assess differences in these NPCs, we performed RNA sequencing (RNA-seq) experiments. We found changes in the levels of 195 transcripts (FC > 2, P-value < 0.05), of which 35 were up-regulated whereas 160 were down-regulated (Fig. 2F and Supplementary Data 3). Among these down-regulated transcripts, GOBP analysis indicated a strong enrichment for factors involved in signal transduction, cell adhesion and extracellular matrix organization (Fig. 2G and Supplementary Data 3). In addition, reduced HTT levels also decreased the expression of modulators of brain development (e.g. the GABA receptor GABRA5), synapse assembly (e.g. the neurotrophic receptor NTRK3), glutamate signaling pathway (e.g. the glutamate receptors GRIA3, GRIN3A, GRIK2) and vesicle fusion/exocytosis (e.g. SYT4, SYT7 and SYTL1, which mediate Ca^{2+}-dependent exocytosis of neurotransmitters) (Fig. 2G and Supplementary Data 3). Notably, NPCs derived from HTT KD hESCs not only exhibited alterations in gene expression but also maintained high levels of H3K9me3 compared with control NPCs (Fig. 2H and I).

To gain insights into the regulatory mechanisms by which HTT regulates H3K9me3 levels, we first asked whether loss of HTT impairs ATF7IP levels. However, we did not find changes in the transcript and protein levels of this chromatin factor upon HTT KD (Fig. 3A and B, Supplementary Material, Table S1 and Supplementary Data 4). Likewise, loss of HTT did not affect the protein levels of SETDB1 (Fig. 3B and Supplementary Material, Table S1). Moreover, co-IP experiments did not show a significant increase in the interaction of ATF7IP with SETDB1 upon HTT KD (Fig. 3C). However, loss of HTT changed the nuclear distribution of ATF7IP, which markedly concentrated in specific areas in contrast to the diffused pattern characteristic of control hESCs (Fig. 3D). In addition, we observed colocalization of SETDB1 with these ATF7IP nuclear dots upon HTT down-regulation (Fig. 3D). Prompted by these results, we examined whether HTT regulates the interactome of ATF7IP. For this purpose, we performed co-IP experiments with anti-ATF7IP antibody in HTT KD hESCs followed by quantitative proteomics (Supplementary Data 5). Remarkably, hierarchical clustering indicated clear differences in the binding partners of ATF7IP upon HTT KD (Supplementary Material, Fig. S5). Whereas the interaction with SETDB1 remained similar, ATF7IP gained interactions with distinct transcriptional repressors upon loss

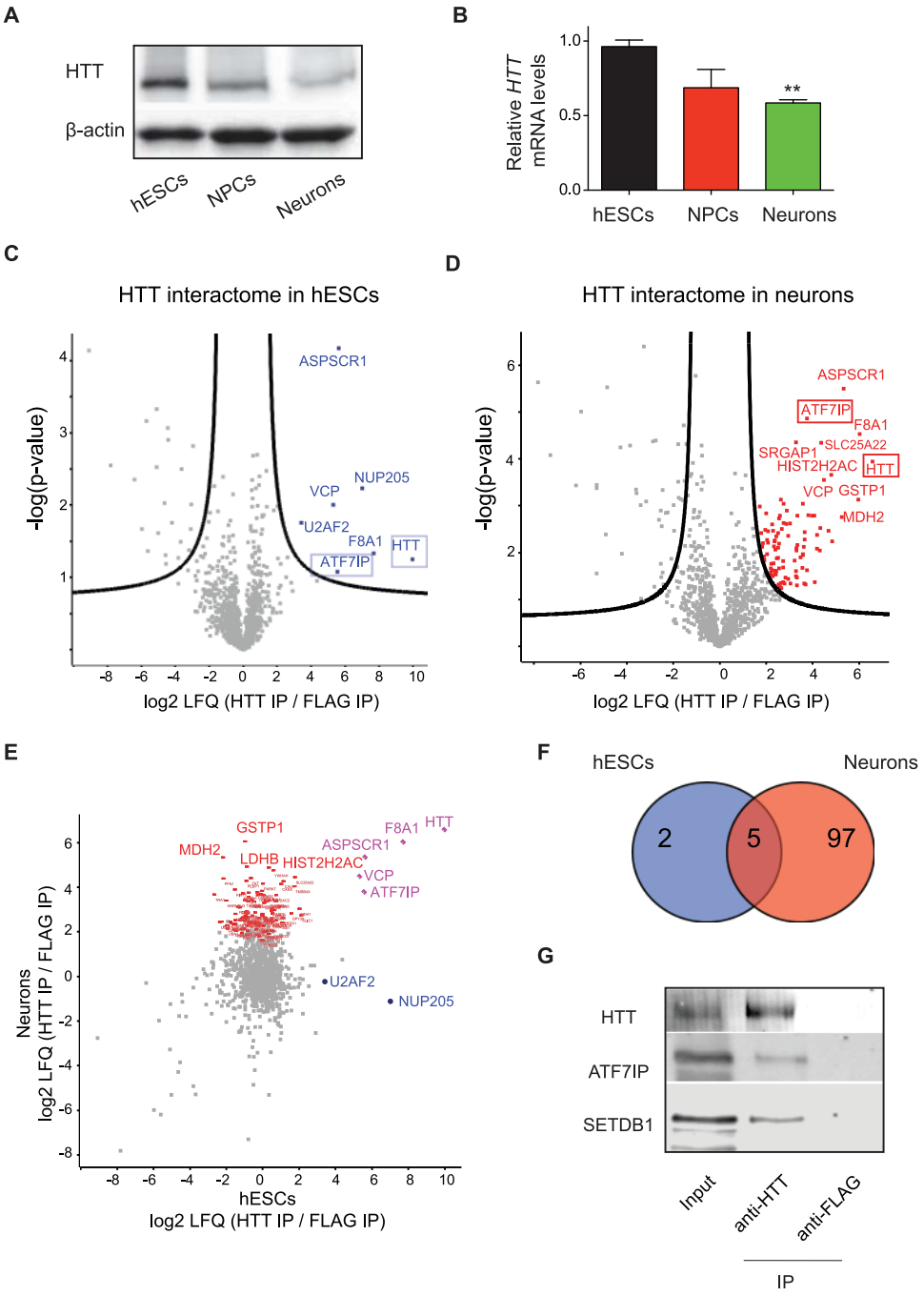

Figure 1. HTT interacts with the chromatin factor ATF7IP in hESCs and neurons. **(A)** Western blot analysis of H9 hESCs and their differentiated counterparts with antibody to HTT. β-actin is the loading control. The images are representative of three independent experiments. **(B)** Quantitative PCR (qPCR) analysis of HTT mRNA levels (mean ± s.e.m. of three independent experiments). Statistical comparisons were made by Student's *t*-test for unpaired samples. *P*-value: ** ($P < 0.01$). **(C)** Volcano plot of HTT interactome in H9 hESCs ($n = 3$). –log (*P*-value) of a two-tailed *t*-test is plotted against the log2 ratio of protein label-free quantification (LFQ) values from co-IP experiments using HTT antibody compared to control co-IP with FLAG antibody. Blue coloured dots beyond the curved lines indicate significance after correction for multiple testing [false discovery rate (FDR) < 0.05 was considered significant]. **(D)** Volcano plot of HTT interactome in neurons ($n = 4$). Red coloured dots beyond the curved lines demonstrate significance after correction for multiple testing (FDR < 0.05 was considered significant). **(E)** Scatterplot of protein enrichments in HTT co-IP from hESCs and neuronal cells. Significant intrinsic interactors in neurons, hESCs as well as common interactors in both cell types are indicated in red, blue and magenta, respectively (FDR < 0.05 was considered significant). **(F)** Venn diagram represents the number of specific and common co-immunoprecipitated proteins with HTT antibody in hESCs and neurons. **(G)** Co-IP with HTT and control FLAG antibodies in H9 hESCs followed by western blot with HTT, ATF7IP and SETDB1 antibodies. The images are representative of three independent experiments.

of HTT which were not detected in control hESCs (Fig. 3E and Supplementary Data 5). Among them, HTT KD triggered the interaction of ATF7IP with DNMT3B, a DNA methyltransferase that establishes DNA methylation patterns in hESCs and development, a process highly coordinated with histone methylation (68). Moreover, HTT down-regulation induced the binding of ATF7IP with SMARCC2, a subunit of the SWI/SNF chromatin remodelling complex that regulates transcriptional

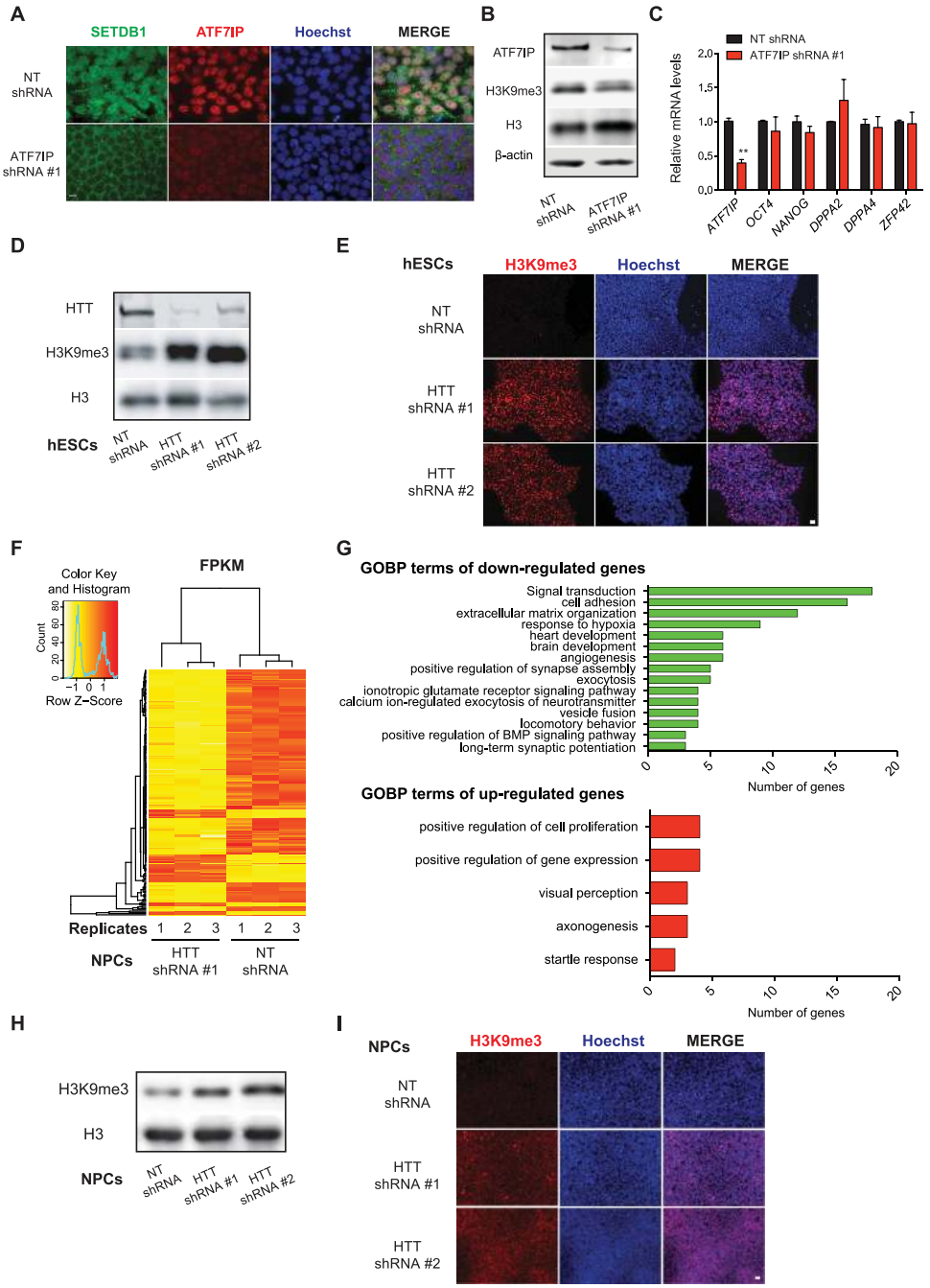

Figure 2. Loss of HTT induces trimethylation of H3K9 in hESCs. (**A**) Immunocytochemistry of H9 hESCs with antibodies to ATF7IP and SETDB1. Hoechst staining was used as a marker of nuclei. Scale bar represents 10 μm. The images are representative of two independent experiments. (**B**) Western blot analysis of H9 hESCs upon ATF7IP KD with antibodies to ATF7IP, H3K9me3, total H3 and β-actin. The images are representative of two independent experiments. (**C**) qPCR analysis of pluripotency markers. Graph (relative expression to NT shRNA H9 hESCs) represents the mean ± s.e.m. of three independent experiments. Statistical comparisons were made by Student's *t*-test for unpaired samples. *P*-value: ** ($P < 0.01$). (**D**) Western blot analysis of H9 hESC lysates with antibodies to HTT, H3K9me3 and total H3. The images are representative of three independent experiments. (**E**) Immunocytochemistry of H9 hESCs with antibody to H3K9me3. Hoechst staining was used as a marker of nuclei. Scale bar represents 20 μm. The images are representative of three independent experiments. (**F**) Heatmap representing differentially expressed transcripts (FC > 2, *P*-value < 0.05) in NPCs derived from HTT KD hESCs identified by RNA-seq analysis ($n = 3$ biological replicates). (**G**) GOBP analysis of down-regulated and up-regulated transcripts in NPCs derived from HTT KD hESCs. For down-regulated transcripts, 15 of the 30 most enriched GOBPs are shown. Please see Supplementary Data 3 for the complete list of enriched GOBP terms. Statistical comparisons with a modified Fisher's exact test (EASE score) below the *P*-value cutoff of 0.05 were considered significant. (**H**) Western blot analysis of NPCs derived from H9 hESCs with antibodies to H3K9me3 and total H3. The images are representative of three independent experiments. (**I**) Immunocytochemistry of H9 NPCs with antibody to H3K9me3. Hoechst staining was used as a marker of nuclei. Scale bar represents 20 μm. The images are representative of three independent experiments.

repression and hESC differentiation (69). Likewise, we observed a strong interaction with protein polybromo-1, a factor that stabilizes the SWI/SNF complex, and SMARCAD1, an SWI/SNF regulator that stimulates heterochromatin formation (70). Upon HTT KD, ATF7IP also interacted with HP1B3, a heterochromatin-binding protein that promotes chromatin condensation and

maintains heterochromatin integrity (71,72). Other interactions of ATF7IP detected only upon HTT down-regulation were the non-histone chromatin-associated protein HMGA1, which mediates the accessibility of protein complexes to DNA during development (73), and WDR82, a regulator of H3K4 methylation (74). Besides these chromatin regulators, ATF7IP also gained interactions with the transcriptional repressor SLTM (75) as well as GATAD2A/GATAD2B factors, which are recruited by the scaffolding MBD2 protein at DNA-methylated sites to promote gene silencing (76). On the contrary, ATF7IP lost the interaction with distinct chromatin and transcriptional regulators upon HTT KD (Fig. 3E and Supplementary Data 5). Among them, we found the histone chaperone NAP1L4 that transfers histones from the cytoplasm to the nucleus (77) as well as RUVBL2, a regulatory component of the histone acetyltransferase TIP60 complex which promotes transcriptional activation (78). Likewise, HTT KD impaired the interaction of ATF7IP with USP7, an enzyme involved in chromatin regulation by promoting the deubiquitination of core subunits of the polycomb repressive complex 1 (PRC1) such as PCGF2 and BMI1 (79). The PRC1 complex promotes chromatin compaction/gene suppression and is required for differentiation of ESCs (80,81). Notably, changes in the interactome of ATF7IP were not associated to dysregulation in the expression of these proteins, as we observed in proteomic analysis of HTT KD hESC lysates (Supplementary Material, Table S1 and Supplementary Data 4). Taken together, our results indicate that HTT inhibits the binding of the ATF7IP-SETDB1 complex with transcriptional repressors and heterochromatin regulators, correlating with reduced formation of H3K9me3.

H3K9me3 marks in hESCs upon HTT KD impair induction of distinct neural genes

Loss of HTT did not impair the levels of pluripotency markers in hESCs (Fig. 4A and B). Moreover, we found no differences in the markers of the distinct germ layers (Fig. 4C). To further assess changes induced by loss of HTT, we analyzed the proteome of hESCs. Besides HTT, other 14 (9 up-regulated, 5 down-regulated) proteins were significantly changed in both independent HTT KD hESC lines (Supplementary Material, Table S2 and Supplementary Data 4). Among them, we found an increase in the levels of laminin subunits (i.e. LAMA1, LAMB1 and LAMC1) and nidogen-1, a protein tightly associated to laminin (Supplementary Material, Table S2 and Supplementary Data 4). Moreover, both HTT KD hESC lines exhibit a significant increase in SUV39H1, a H3K9 methyltransferase (82,83) that can form multimeric complexes with other H3K9 methylases such as SETDB1 (84) and, therefore, could contribute to the aberrant H3K9me3 levels observed in HTT KD hESCs.

Although quantitative proteomics revealed moderate changes induced by loss of HTT in hESCs, it also presents important limitations for our study. For instance, this approach could restrict the quantification of transcription factors as well as low abundant proteins in hESCs which expression is triggered during differentiation. We hypothesized that H3K9me3 repressive marks could further decrease the expression of these genes in hESCs or, more importantly, diminish their induction during differentiation. To test this hypothesis, we performed chromatin immunoprecipitation-sequencing (ChIP-seq) assays of hESCs using an antibody to H3K9me3 (Supplementary Data 6). We found a >1.5-FC enrichment (P-value < 0.05) for H3K9me3 marks in 3244 regions upon HTT KD in hESCs (Fig. 4D and Supplementary Data 6). Although most of them were not associated with genes, 68 contained gene regions distributed in 19 exons, 19 introns, 29 promoters and 1 transcription termination site (Fig. 4E, Supplementary Data 6 and 7). GO term analysis of these genes indicated the strongest enrichment for factors involved in transcriptional regulation (Supplementary Material, Fig. S6). These regulators include three zinc finger proteins (ZNF135, ZNF572, ZNF844), one transcription elongation factor (TCEB3CL) and three developmental transcription factors (DLX3, ASCL2, GBX1). DLX3 contributes to ectoderm differentiation (85). ASCL2 is a proneural factor involved in the determination of neuronal precursors of the nervous system and its transcription is regulated via histone modifications during neural differentiation from hESCs (86). GBX1 is highly expressed in the neuroectoderm and regulates the positioning of the midbrain–hindbrain boundary organizer in the early neural plate, affecting forebrain and midbrain formation (87). Besides these transcription factors, we found an enrichment for H3K9me3 in genes involved in nervous system formation, neuronal function, neurotransmission and synapse genesis/stabilization [i.e. CELSR1, CPEB1 (88), SMC1B, ADRA2B, MRGPRX3]. Dysfunctions in calcium homeostasis are one of the major alterations observed in HD neurons (39,89). Interestingly, we have found H3K9me3 enrichment in genes involved in calcium metabolism such as OTOP1, ARPP21 [an inhibitor of calmodulin-dependent enzymes in striatal neurons (90)] and OPRD1, which regulates neurotransmitter release by modulating calcium currents (91). Prompted by these findings, we asked whether H3K9me3 marks induced by HTT KD results in decreased expression of these genes. In particular, we focused on the transcription factors DLX3, ASCL2 and GBX1 because of their important role in development. Notably, we did not observe significant changes in the expression of these factors at the hESC stage (Fig. 4F). With the exception of ASCL2 (FC = −1.29), early NPCs from HTT KD hESCs (10 days of neural induction) did not exhibit a significant decreased expression of these transcription factors when compared with control NPCs by RNA-seq (Supplementary Data 3). However, it is important to note that the expression of these genes was still marginal at the early NPC stage, as reflected by their low FPKM (Fragment Per Kilobase Million) values (Supplementary Data 3). Indeed, we confirmed by quantitative PCRthat the expression of ASCL2 and GBX1 was not induced in control NPCs at this early stage when compared with hESCs (Supplementary Material, Fig. S7). For this reason, we further differentiated them (20 days on neural induction treatment) to obtain NPCs with the capacity to generate terminally differentiated neurons. At this stage, control NPCs exhibited induced expression of ASCL2, GBX1 and DLX3 when compared to hESCs (Fig. 4G). Thus, we asked whether H3K9me3 marks in these genes at the hESC stage impair their induction. Indeed, loss of HTT in hESCs diminished their ability to induce the expression of ASCL2, GBX1 and DLX3 during differentiation (Fig. 4G). In addition, we confirmed that HTT KD in hESCs also resulted in decreased expression of other H3K9me3-enriched genes after 20 days of neural induction (i.e. SMC1B, ADGRB1) (Supplementary Material, Fig. S8). On the contrary, we could not detect H3K9me3 enrichment in these genes when HTT KD hESCs were differentiated into NPCs for 20 days, as the increased H3K9me3 peaks were essentially distributed in intergenic regions in these cells (Supplementary Data 8). Thus, our data indicate that H3K9me3 alterations at earlier stages affect the induction of specific neural genes during the differentiation process. We then assessed whether NPCs (20 days neural induction) derived from HTT KD hESCs retain their ability to terminally differentiate into neurons.

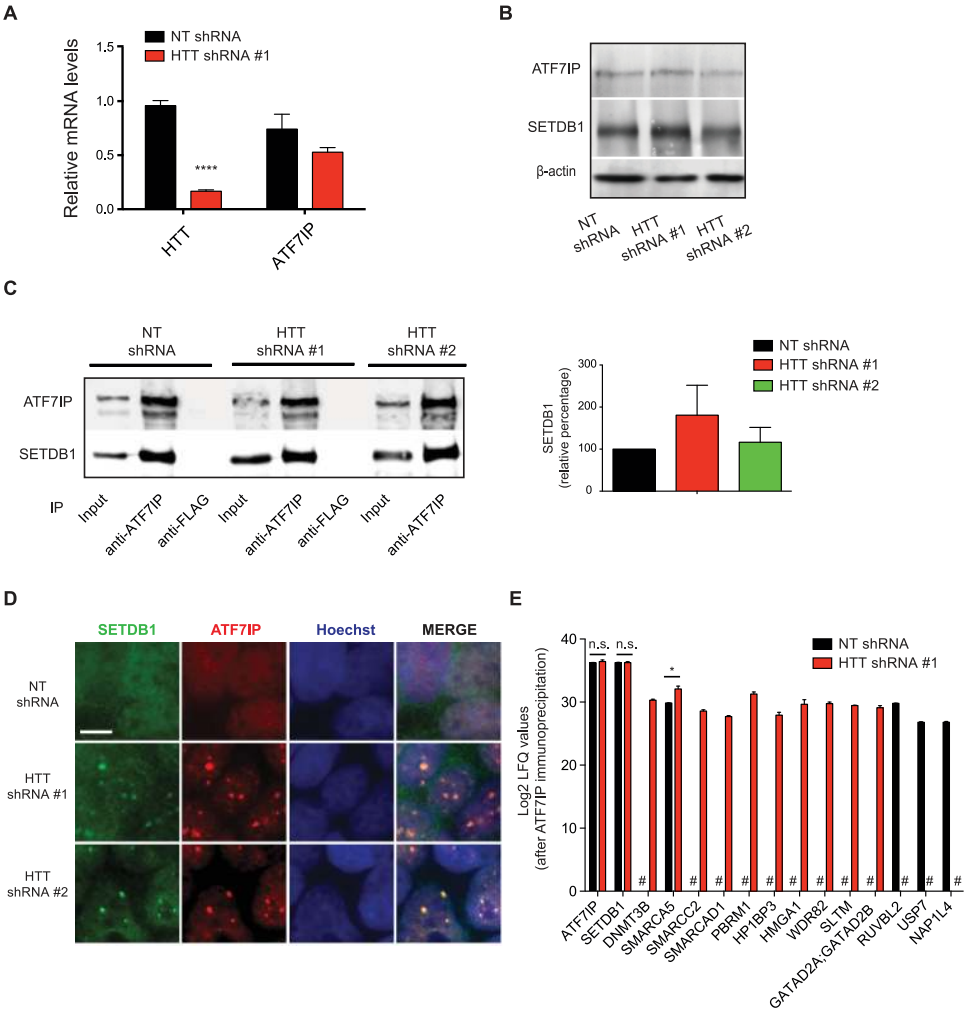

Figure 3. HTT inhibits the interaction of ATF7IP with heterochromatin factors. (**A**) qPCR analysis of HTT and ATF7IP levels. Graph (relative expression to NT shRNA H9 hESCs) represents the mean ± s.e.m. of three independent experiments. Statistical comparisons were made by Student's *t*-test for unpaired samples [*P*-value: ****($P < 0.0001$)]. (**B**) Western blot analysis of H9 hESCs with antibodies to ATF7IP and SETDB1. β-actin is the loading control. The images are representative of four independent experiments. (**C**) Co-ip with ATF7IP and FLAG antibodies in H9 hESCs followed by western blot with antibodies to ATF7IP and SETDB1. The graph represents the relative percentage values to NT shRNA-hESCs of co-immunoprecipitated SETDB1 corrected for immunoprecipitated ATF7IP using anti-ATF7IP antibody (mean ± s.e.m. of three independent experiments). Statistical comparisons were made by Student's *t*-test for unpaired samples and no significant differences were found. (**D**) Immunocytochemistry of H9 hESCs with antibody to SETDB1 and ATF7IP. Hoechst staining was used as a marker of nuclei. Scale bar represents 10 µm. On the right, a higher magnification of representative cells for the different conditions is presented. The images are representative of three independent experiments. (**E**) log2 LFQ values from co-IP experiments using anti-ATF7IP antibody in NT shRNA and HTT shRNA #1-hESCs ($n = 4$). For each protein, the bar represents the mean ± s.e.m. when the signal was detected in at least three replicates of the same condition. The # indicates that signal was not detected in any of the replicates. Statistical comparisons were made by Student's *t*-test. *P*-value: *($P < 0.05$).

Although NPCs could differentiate into MAP2-positive neuronal cells (Supplementary Material, Fig. S9A), the neurons expressed dysregulated levels of neuronal genes such as synapsin or the GABA receptor GABBR2 (Supplementary Material, Fig. S9B). Moreover, they retained abnormal high expression of the neural marker PAX6 (Supplementary Material, Fig. 9A–C). Altogether, these results suggest that loss of HTT dysregulates H3K9me3 in hESCs, a process that could contribute to altered gene expression upon neural differentiation and affect neurogenesis.

Mutant polyQ-expanded stretch impairs HTT-ATF7IP interaction

Since our results indicate that HTT interacts with ATF7IP to regulate H3K9me3, we asked whether polyQ-expanded mutations alter this normal function of HTT. To assess this hypothesis, we examined iPSCs derived from an individual with juvenile onset HD (92). These HD-iPSCs express one mutant copy of HTT (Q71) but also one normal copy (Q19) (Fig. 5A) (92,93), allowing for direct assessment of differences between wild-type and mutant HTT in their interaction with the ATF7IP-SETDB1 complex. For this purpose, we performed co-IP experiments using either an antibody against total HTT or polyQ-expanded HTT (94). After we confirmed the later antibody only immunoprecipitated mutant HTT, we performed western blot against ATF7IP and SETDB1 (Fig. 5A). Strikingly, we could not detect ATF7IP and SETDB1 in polyQ-expanded HTT pulldowns. On the contrary, anti-total HTT antibody co-immunoprecipitated these chromatin regulators in HD-iPSCs (Fig. 5A), indicating that mutations in the polyQ stretch impair HTT interaction with ATF7IP. With the increased trimethylation of H3K9 in brain tissues of HD patients and mouse models (52–55), we asked whether HD-iPSCs also

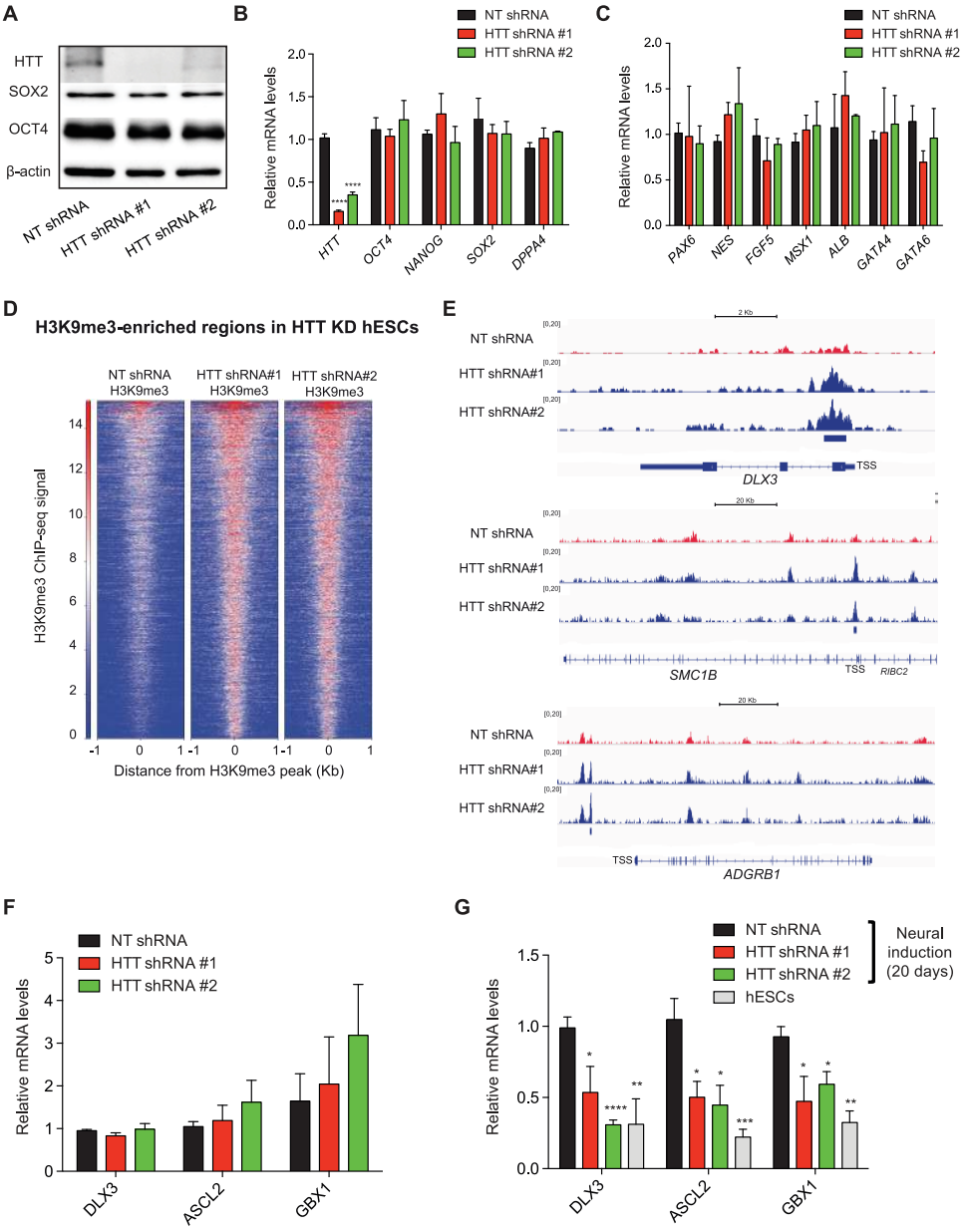

Figure 4. Altered H3K9me3 marks in hESCs upon HTT KD impairs the induction of distinct neural genes. **(A)** Western blot analysis of H9 hESC lysates with antibodies to HTT, OCT4 and SOX2. β-Actin is the loading control. **(B)** The KD of HTT does not change the mRNA levels of pluripotency markers. Graph [relative expression to non-targeting (NT) shRNA H9 hESCs] represents the mean ± s.e.m. ($n = 9$). **(C)** qPCR analysis of ectodermal (PAX6, NES, FGF5), mesodermal (MSX1) and endodermal (ALB, GATA4, GATA6) germ layer markers. Graph (relative expression to NT shRNA hESCs) represents the mean ± s.e.m. ($n = 8$). **(D)** Significant H3K9me3-enriched regions (>2-fold, $P < 0.05$) upon HTT KD identified by ChIP-seq experiments. The images are representative of two independent experiments. **(E)** H3K9me3 ChIP-seq profiles of DLX3, SMC1B and ADGRB1 generated in NT and HTT shRNA hESCs. **(F)** qPCR analysis of H9 hESCs. Graph (relative expression to NT shRNA) represents the mean ± s.e.m. of three independent experiments. **(G)** qPCR analysis after 20 days of neural induction. Graph (relative expression to NT shRNA NPCs) represents the mean ± s.e.m. of three independent experiments. All the statistical comparisons were made by Student's *t*-test for unpaired samples. *P*-value: *($P < 0.05$), **($P < 0.01$), ***($P < 0.001$), ****($P < 0.0001$).

exhibit impaired H3K9me3 levels. Similar to HTT KD hESCs, Q71 HD-iPSCs had increased H3K9me3 levels when compared to control iPSCs (Fig. 5B). Likewise, an independent HD-iPSC line expressing normal HTT (Q18) and a distinct mutant HTT allele (Q180) (38,92,93) also exhibited higher H3K9me3 (Fig. 5B). When HD-iPSCs were differentiated into NPCs (20 days of neural differentiation), these cells exhibited dramatic alterations in gene expression compared with control NPCs (Supplementary Data 9). RNA-seq experiments revealed that 2171 transcripts were up-regulated in HD-NPCs (Q180) (FC > 2, *P*-value < 0.05), of which GOBP analysis indicated the strongest enrichment for genes involved in transcriptional regulation, organismal development and cell adhesion (Fig. 5C and Supplementary Data 9). On the contrary, the steady-state levels of 2143 transcripts were down-regulated with GOBP enrichment for factors involved in signal transduction, cell adhesion and extracellular matrix organization (Fig. 5C and Supplementary Data 9). Moreover, these down-regulated genes were also enriched for modulators of organismal development, cell differentiation, brain development (e.g. the transcription factor FOXG1 and SYT4), axon guidance

(e.g. NTRK1), chemical synaptic transmission and regulation of Ca^{2+} cytosolic levels (e.g. G-protein coupled receptors GNA15 and GPR6) (Fig. 5C and Supplementary Data 9). Among these down-regulated transcripts, we found ASCL2 and DLX3, but not GBX1 or SMC1B (Supplementary Data 9).

Prompted by these findings, we examined whether loss of ATF7IP diminishes trimethylation of H3K9 in NPCs derived from HD-iPSCs. Indeed, we found that ATF7IP KD after differentiation is sufficient to reduce H3K9me3 levels in HD-NPCs (Fig. 6A). Since differentiation of HD-iPSCs generates NPCs that already present HD-related changes (38,39), one step further was to reduce H3K9me3 levels at the pluripotent state. Notably, KD of ATF7IP diminished H3K9me3 levels in HD-iPSCs (Figs 6B–D) without affecting the expression of distinct pluripotency markers (Supplementary Material, Fig. S10). To further characterize the effects of ATF7IP KD in HD-iPSCs, we examined mutant HTT aggregates. Under normal conditions, HD-iPSCs suppress mutant HTT aggregation through their intrinsic proteasome and protein folding activities, which are enhanced in these cells (2,38,93,95–97). However, dysregulation of either the ubiquitin proteasome system or the chaperone network triggers mutant HTT aggregation in these cells (2,38,93,95–97). On the contrary, we did not detect mutant HTT aggregates in HD-iPSCs upon ATF7IP KD, indicating that this treatment does not have deleterious effects on HTT aggregation (Supplementary Material, Fig. S11). Prompted by these results, we asked whether KD of ATF7IP at the pluripotent stage can correct alterations in gene expression of NPCs differentiated from HD-iPSCs. For this purpose, we induced neural differentiation (20 days) of ATF7IP KD HD-iPSCs and analyzed their transcriptome (Supplementary Data 10). Among the 2171 transcripts up-regulated in HD-NPCs compared with control NPCs, ATF7IP KD significantly (FC $>$ 2, P-value $<$ 0.05) decreased the levels of 1263 transcripts in HD-NPCs whereas 34 transcripts were further up-regulated (Fig. 6E and Supplementary Data 11). Regarding the 2143 transcripts down-regulated in HD-NPCs compared with control NPCs, ATF7IP KD significantly rescued the expression of 852 transcripts (e.g. DLX3) whereas only 44 transcripts were further down-regulated (Fig. 6E and Supplementary Data 11). Notably, we found that ATF7IP KD rescues the expression of PPP1R1B (also known as DARPP32) (Supplementary Data 11), which is highly expressed in striatal neurons and markedly decreased in the brains of HD patients and mouse models (43). Altogether, our data suggest that modulation of ATF7IP in HD-iPSCs can ameliorate alterations in H3K9me3 levels and reduce gene expression changes in their NPC counterparts.

Discussion

The ubiquitous subcellular localization of HTT does not facilitate the definition of its function. Multiple roles have been described for wild-type HTT. For instance, HTT is involved in vesicular transport (98–100), mitotic spindle orientation (22) and regulation of selective autophagy (101). Besides a gain of function in HTT, loss of normal function could also contribute to HD (3,4). Thus, defining its normal function is of central importance. In these lines, HTT modulates gene expression by binding numerous transcription factors and regulators such as the cAMP-response element-binding protein, specificity-protein 1, neuroD1, p53 or the nuclear factor-κB (NF-κB) (4). Loss of function of HTT could explain the transcriptional dysregulation observed in postmortem HD brains and mouse models (4,40). Moreover, epigenetic marks including DNA methylation and histone modifications are impaired in both HD patients and organismal models (44). Studies in mESCs supported a role of HTT in the regulation of their epigenetic landscape. In these cells, HTT facilitates trimethylation of H3K27 by the chromatin regulator polycomb repressive complex 2 (PRC2), a mechanism further induced by a gain of function of the mutant HTT (102). Moreover, expression of polyQ-expanded HTT in mESCs impairs H3K4me3 deposition at active loci (49). Neural cultures from HD patient-iPSCs also have alterations in H3K4me3 and H3K27ac, affecting the expression of distinct neurodevelopmental factors (39).

Here we find that HTT interacts with the ATF7IP-SETDB1 complex, a key regulator of H3K9me3. Our results indicate that the high expression of HTT in hESCs blocks the interaction of ATF7IP-SETDB1 with specific regulators of heterochromatin and transcriptional repression, a central process to induce H3K9me3 at heterochromatin formation sites (59,60,63,64). Conversely, loss of HTT facilitates trimethylation of H3K9 in hESCs, which is normally reduced in these cells when compared to their differentiated counterparts (57,58). As such, HTT is required to maintain low levels of H3K9me3 in hESCs. Although H3K9me3 deposition in genes encoding for neurodevelopmental factors does not affect their low expression in hESCs, it correlates with their down-regulated induction during neural differentiation. Thus, HTT allows for hESC differentiation into neural progenitors with normal expression of distinct neurodevelopmental factors, including ASCL2 and GBX1. It will be fascinating to examine whether the effects of HTT on ATF7IP also modulate H3K4me3 and H3K27me3 alterations induced by loss of HTT in ESCs. In these lines, we found that HTT KD induces ATF7IP interaction with WDR82, a regulator of H3K4me3. Whereas HTT modulates H3K27me3 levels via PRC2 in ESCs, we did not observe ATF7IP interaction with the main components of this complex (i.e. SUZ12, EED, EZH1/2 and histone-binding protein RBBP4) in control or HTT KD hESCs (Supplementary Data 5). Thus, HTT may regulate the epigenetic landscape of pluripotent cells via distinct mechanisms. Although PRC2 is required for the initial targeting via H3K27me3 of genomic regions to be silenced, the PRC1 complex stabilizes this silencing promoting chromatin compaction and gene suppression (103). Notably, we found that HTT impairs the binding of ATF7IP to USP7, a deubiquitinating enzyme which interacts with distinct subunits of the PRC1 complex modulating transcriptional repression (79). However, we did not detect interaction of ATF7IP with core subunits or the PRC1 complex.

Transcriptional dysregulation contributes to HD pathogenesis (40,43,44). Multiple studies *in vitro* and *in vivo* support a direct link of epigenetic alterations in the gene expression changes associated to HD (40–48). For instance, H3K4me3 dysregulation alters the expression of genes involved in neuronal function (42,48). H3K27ac marks are down-regulated in mouse HD models and correlate with down-regulated expression of modulators of neuronal plasticity and transmission (41). Remarkably, inhibitors of histone deacetylase can ameliorate HD-related changes (43). Thus, identifying mechanisms underlying epigenetic alterations in HD and their link with transcriptional dysregulation is of central interest. Although H3K9me3 levels are up-regulated in the brain of HD patients and mouse models (52–55), relatively little is known about the link between these modifications, transcriptional dysregulation and HD pathogenesis. Notably, polyQ-expanded HTT lacks the ability to interact with the ATF7IP-SETDB1 complex, a process that could contribute to the dysregulated levels of H3K9me3 in

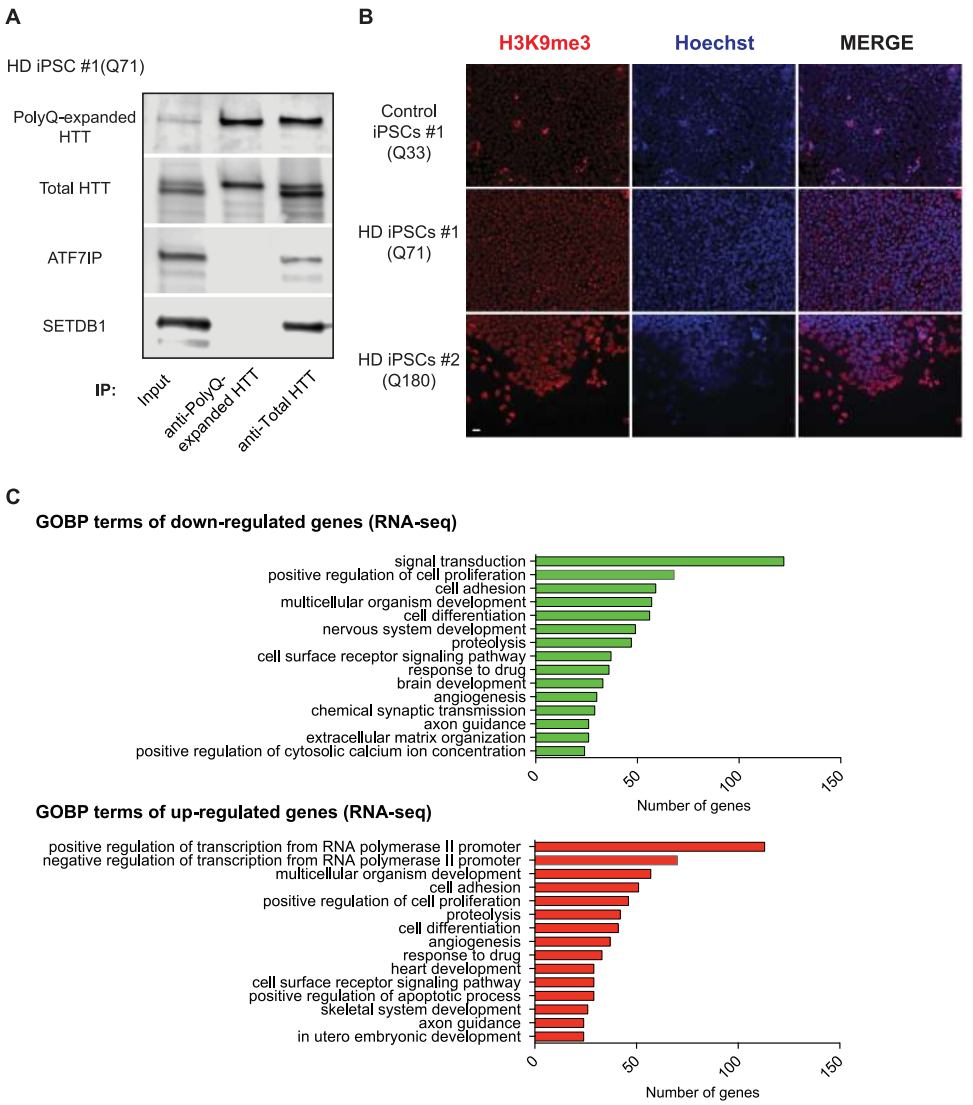

Figure 5. Mutations in HTT reduce its interaction with ATF7IP and induce H3K9me3. (**A**) Co-ip with anti-polyQ-expanded HTT and anti-total HTT antibodies in HD iPSC line #1 (Q71) followed by western blot with antibodies to polyQ-expanded HTT, total HTT, ATF7IP and SETDB1. The images are representative of three independent experiments. (**B**) Immunocytochemistry of control iPSCs #1 (Q33), HD-iPSCs #1 (Q71) and HD-iPSCs #1 (Q180) with antibody to H3K9me3. Hoechst staining was used as a marker of nuclei. Scale bar represents 20 µm. The images are representative of three independent experiments. (**C**) GOBP analysis of down-regulated and up-regulated transcripts in NPCs derived from HD-iPSCs #1 (Q180) after 20 days of neural induction compared with NPCs from control iPSCs #1 (Q33). About 15 of the 30 most enriched GOBPs are shown. Please see Supplementary Data 9 for complete list of enriched GOBP terms. Statistical comparisons with a P-value < 0.05 (modified Fisher's exact test) were considered significant.

iPSCs derived from HD patients. When these cells differentiate into NPCs, they exhibit down-regulated levels of numerous genes enriched in biological processes linked with nervous system development and neuronal function, including axon guidance and chemical synaptic transmission as previously identified in disease models (43). Although these HD-NPCs present down-regulated expression of ASCL2 and DLX3, they do not present decreased levels of all the neurodevelopmental factors observed in HTT KD cells. It is important to note that the available HD-iPSC lines, including the ones used in this study, not only express mutant HTT but also one normal copy (38,93,104), which could be sufficient to reduce the impact of diminished mutant HTT interaction with ATF7IP-SETDB1. Moreover, these results support the findings in HD patients and disease mouse models, which do not manifest developmental phenotypes at the same extent than HTT knockout models (3,21,25,26). Nevertheless, our data indicate that polyQ-expanded mutations could alter the ability of HTT to regulate ATF7IP-SETDB1, impairing H3K9me3 levels in iPSCs. Conversely, loss of ATF7IP in HD-iPSCs reduces trimethylation of H3K9 and corrects numerous gene expression changes in HD-NPCs. Among them, we found that ATF7IP KD rescues the down-regulated expression of DLX3 and PPP1R1B/DARPP32, which is dysregulated in HD patients and mouse models (43). Whether diminished interaction of mutant HTT with ATF7IP-SETDB1 contributes to HD is unknown. Remarkably, a recent study reported that genetic variations in ATF7IP correlate with age of onset in HD patients (105). Thus, it will be fascinating to examine the link between HTT, ATF7IP and epigenetic dysregulation in HD.

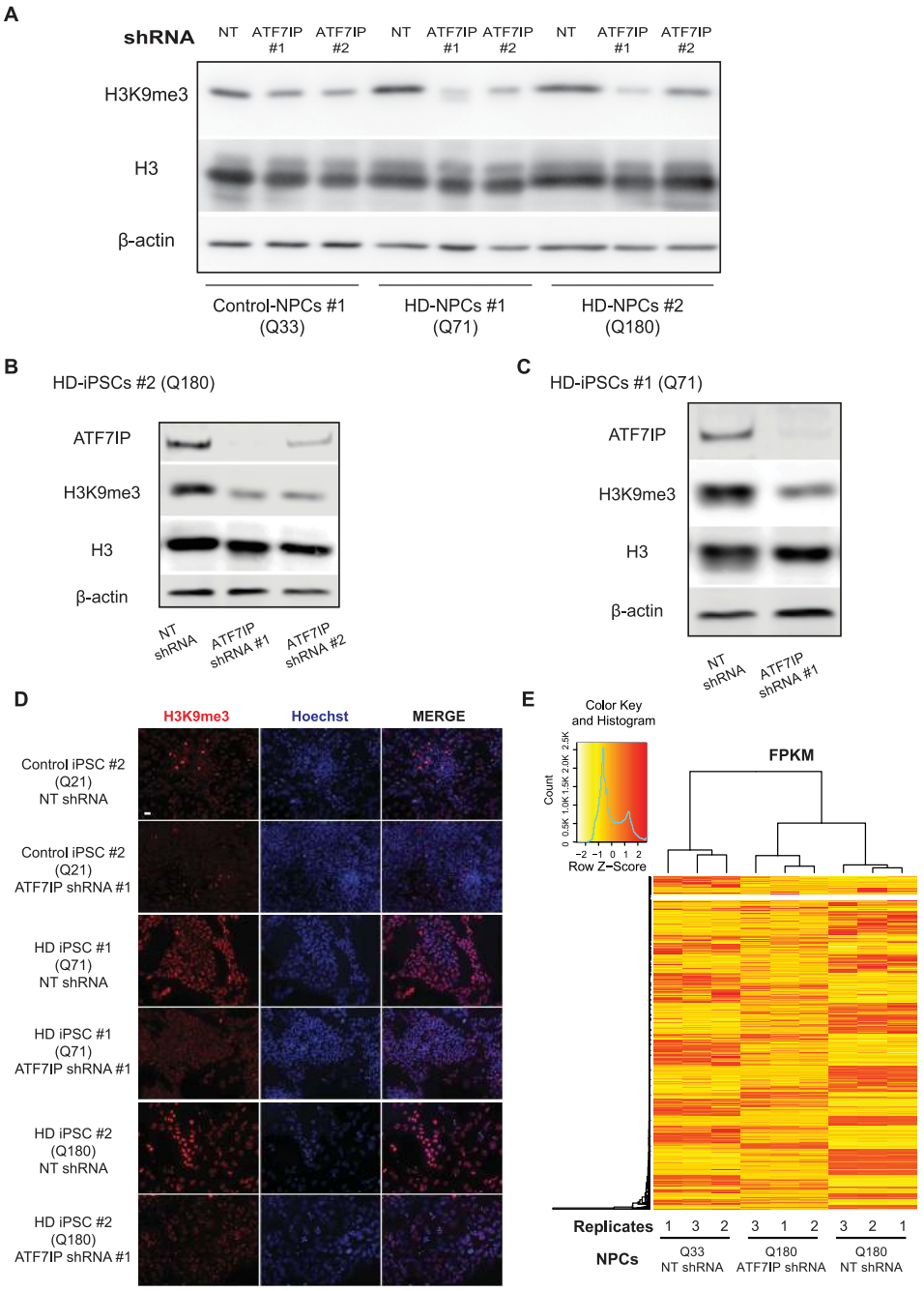

Figure 6. KD of ATF7IP reduces H3K9me3 levels in HD-iPSCs. (**A**) KD of ATF7IP in NPCs (20 days of neural induction) decreases H3K9me3 levels as assessed by western blot experiments. The images are representative of two independent experiments. (**B**) Western blot analysis of HD-iPSC line #2 (Q180) lysates with antibodies to H3K9me3 and total H3. β-actin is the loading control. The images are representative of three independent experiments. (**C**) Western blot analysis of HD-iPSC line #1 (Q71) lysates with antibodies to H3K9me3 and total H3. β-Actin is the loading control. Images are representative of two independent experiments. (**D**) Immunocytochemistry of control iPSC line #3 (Q21), HD-iPSC line #1 (Q71) and HD-iPSC line #2 (Q180) with antibody to H3K9me3. Hoechst staining was used as a marker of nuclei. Scale bar represents 20 μm. Images are representative of three independent experiments. (**E**) Heatmap representing transcripts differentially expressed in NT shRNA HD-NPCs (Q180) versus NT shRNA control-NPCs (Q33) ($P < 0.05$, FC > 2). The heatmap also presents the levels of these transcripts in ATF7IP shRNA HD-NPCs (Q180) for comparison. NPCs were induced during 20 days on neural media ($n = 3$ biological replicates).

Materials and Methods

hESC/iPSC culture and differentiation

The H9 (WA09) and H1 (WA01) hESC lines were obtained from the WiCell Research Institute. ND36997 (control iPSC line #1, Q33), ND42242 (control iPSC line #2, Q21) and ND36999 (HD-iPSC line #2, Q180) were obtained from NINDS Human Cell and Data Repository through Coriell Institute. These iPSC lines were generated and fully characterized for pluripotency in (38). HD-iPSC (Q71) line #1 was a gift from G.Q. Daley and fully characterized for pluripotency in (92). Both HD-iPSC (Q71) and HD-iPSC (Q180) lines were derived from individuals with juvenile onset HD.

hESCs and iPSCs were maintained on Geltrex (Thermo Fisher Scientific, Darmstadt, Germany) using mTeSR1 media (Stem Cell Technologies, Cologne, Germany). Undifferentiated hESC/iPSC colonies were passaged using a solution of dispase (2 mg ml^{-1}) and scraping the colonies with a glass pipette. All the cell lines used in this study were tested for mycoplasma contamination at least once every three weeks. No mycoplasma contamination was detected. Research involving hESC lines was performed with approval of the German Federal competent authority (Robert Koch Institute).

We induced neural differentiation of hESCs/iPSCs with STEMdiff Neural Induction Medium (Stem Cell Technologies) following the monolayer culture method as previously described (106). Undifferentiated cells were rinsed once with Phosphate Buffered Saline (PBS) and then we added 1 ml of Gentle Dissociation Reagent (Stem Cell Technologies) for 10 min. After the incubation period, we gently dislodged hESCs/iPSCs and add 2 ml of Dulbecco's Modified Eagle Medium (DMEM)-F12 (Thermo Fisher Scientific) + 10 μM ROCK inhibitor (Abcam, Cambridge, UK). Then, we centrifuged cells at 300 g for 10 min. hESCs/iPSCs were resuspended on STEMdiff Neural Induction Medium + 10 μM ROCK inhibitor and plated on polyornithine (15 μg ml^{-1})/laminin (10 μg ml^{-1})-coated plates at a density of 200 000 cells cm^{-2}.

For pan-neuronal differentiation, NPCs derived from hESCs were cultured on neural induction media for at least 20 days. Then, NPCs were dissociated with Accutase (Stem Cell Technologies) and transferred to polyornithine/laminin-coated plates in neuronal differentiation medium consisting of DMEM/F12, B27, N2 (Thermo Fisher Scientific), 1 μg ml^{-1} laminin (Thermo Fisher Scientific), 20 ng ml^{-1} GDNF (Peprotech, Hamburg, Germany), 20 ng ml^{-1} BDNF (Peprotech), 200 nM ascorbic acid (Sigma, Hamburg, Germany) and 1 mM dibutyryl-cyclic AMP (Sigma) (107). Cells were differentiated for 1 month, with weekly feeding of neuronal differentiation medium.

Lentiviral infection of hESCs/iPSCs

Lentivirus (LV)-non-targeting short hairpin (shRNA) control, LV-HTT shRNA #1 (TRCN0000322961), LV-HTT shRNA #2 (TRCN0000019869), LV-ATF7IP shRNA #1 (TRCN0000020827) and LV-ATF7IP shRNA #2 (TRCN0000338504) in pLKO.1-puro vector were obtained from Mission shRNA (Sigma). To obtain shRNA stable lines (108), hESC/iPSC colonies growing on Geltrex were incubated with mTesR1 medium containing 10 μM ROCK inhibitor for 1 h and individualized using Accutase. Fifty thousand cells were infected with 20 μl of concentrated LV in the presence of 10 μM ROCK inhibitor for 1 h. Cell suspension was centrifuged to remove virus, passed through a mesh of 40 μM to obtain individual cells, and plated back on a feeder layer of mitotically inactive mouse embryonic fibroblasts (MEFs) in DMEM/F12, 20% knockout serum replacement (Thermo Fisher Scientific), 0.1 mM non-essential amino acids, 1 mM L-glutamine, β-mercaptoethanol and 10 ng ml^{-1} bFGF (Joint Protein Central, Incheon, Korea) supplemented with 10 μM ROCK inhibitor. After several days in culture, small hESC/iPSC colonies arose. Then, we performed 1 μg ml^{-1} puromycin selection during 2 days and colonies were manually passaged onto fresh MEFs to establish new hESC/iPSC stable lines.

Sample preparation for quantitative proteomics and analysis

For the comparison between control and HTT KD H9 hESCs, we performed label-free quantitative (LFQ) proteomics (Supplementary Data 4). Cells were collected in urea buffer [8 M urea, 50 mM ammonium bicarbonate and 1× complete protease inhibitor mix with EDTA (Roche, Berlin, Germany)], homogenized with a syringe and cleared using centrifugation (16 000 g, 20 min). Supernatants were reduced (1 mM DTT, 30 min); alkylated [5 mM iodoacetamide (IAA), 45 min] and digested with trypsin at a 1:100 w/w ratio after diluting urea concentration to 2 M. The day after, samples were cleared (16 000 g, 20 min) and supernatant was acidified. Peptides were cleaned up using stage tip extraction (109). The liquid chromatography tandem mass spectrometry equipment consisted out of an EASY nLC 1000 coupled to the quadrupole-based QExactive instrument (Thermo Fisher Scientific) via a nano-spray electro-ionization source. Peptides were separated on an in-house packed 50 cm column (1.9 μm C18 beads, Dr Maisch) using a binary buffer system: (A) 0.1% formic acid and (B) 0.1% formic acid in acetonitrile (ACN). The content of buffer B was raised from 7 to 23% within 120 min and then increased to 45% within 10 min. Then, buffer B fraction was raised to 80% within 5 min and held for further 5 min after which it was decreased to 5% within 2 min and held there for further 3 min before the next sample was loaded on the column. Eluting peptides were ionized by an applied voltage of 2.2 kV. The capillary temperature was 275°C and the S-lens RF level was set to 60. MS1 spectra were acquired using a resolution of 70 000 (at 200 m/z), an automatic gain control (AGC) target of 3e6 and a maximum injection time of 20 ms in a scan range of 300–1750 Th. In a data dependent mode, the 10 most intense peaks were selected for isolation and fragmentation in the HCD cell using a normalized collision energy of 25 at an isolation window of 2.1 Th. Dynamic exclusion was enabled and set to 20 s. We used the following MS/MS scan properties: 17.500 resolution at 200 m/z, an AGC target of 5e5 and a maximum injection time of 60 ms. All label-free proteomics data sets were analyzed with the MaxQuant software (release 1.5.3.8). We employed the LFQ mode (110) and used MaxQuant default settings for protein identification and LFQ quantification. All downstream analyses were carried out on LFQ values with Perseus (v. 1.5.2.4) (111).

Protein immunoprecipitation for interactome analysis

Cells were lysed in modified Radioimmunoprecipitation assay (RIPA) buffer [50 mM Tris–HCl (pH 7.4), 150 mM NaCl, 1% IgPal, 0.25% sodium deoxycholate, 1 mM EDTA, 1 mM PMSF] supplemented with protease inhibitor (Roche). Lysates were centrifuged at 10 000 g for 10 min at 4°C. Then, the supernatant was collected and incubated with total HTT antibody (Cell Signaling, #5656, 1:50), polyQ-expanded HTT antibody (DSHB, MW1, 1:50) or ATF7IP antibody (Proteintech, Manchester, UK, 14699-1-AP, 1:50) for 30 min and subsequently with 100 μl Protein A beads (Miltenyi, Bergisch Gladbach, Germany) for 1 h on the overhead shaker at 4°C. As a control, the same amount of protein was incubated with anti-FLAG antibody (SIGMA, F7425, 1:100) in parallel. After this incubation, supernatants were subjected to magnetic column purification. Three washes were performed using wash buffer 1 [containing 50 mM Tris–HCl (pH 7.4), 150 mM NaCl, 5% glycerol and 0.05% IgPal]. Next, columns were washed five times with wash buffer 2 [containing 50 mM Tris–HCl (pH 7.4), 150 mM NaCl]. Then, columns were subjected to in-column tryptic digestion containing 7.5 mM ammonium bicarbonate, 2 M urea, 1 mM DTT and 5 ng ml^{-1} trypsin. Digested peptides were eluted using two times 50 μl of elution buffer 1 containing 2 M urea, 7.5 mM Ambic and 5 m IAA. Digests were incubated overnight at room temperature with mild shaking in the dark.

Samples were stage tipped the next day for LFQ proteomics and analyzed with MaxQuant software. The downstream analyses were carried out on LFQ values with Perseus (v. 1.5.2.4). For co-IP assays followed by western blot, the pellet was incubated after the washing steps with 2× Laemmli Buffer, boiled for 5 min and centrifuged 5 min at maximum speed. The supernatant was taken and loaded onto a sodium dodecyl sulfate–polyacrylamide gel electrophoresis (SDS–PAGE) gel for western blot analysis.

ChIP-sequencing

Cells were crosslinked with 1% formaldehyde for 10 min at room temperature. Crosslinked cells were quenched with 0, 125 M glycine for 10 min at room temperature and then scraped and transferred to a 15 ml conical tube on ice. ChIP experiments from NPCs were performed as described in (112). Regarding H9 hESCs, cells were centrifuged for 5 min at 4°C followed by two washing steps with 5 ml PBS 1×/PMSF 1 mM as previously described (113). H9 hESCs were then resuspended sequentially in three different lysis buffers [lysis buffer 1: 50 mM Hepes, 140 mM NaCL, 1 mM EDTA, 10% glycerol, 0.5% NP-40, 0.25% TX-100 and protease inhibitor (Roche); lysis buffer 2: 10 mM Tris, 200 mM NaCL, 1 mM EDTA, 0.5 mM EGTA; lysis buffer 3: 10 mM Tris, 100 mM NaCL, 1 mM EDTA, 0.5 mM EGTA, 0.1% Na-Deoxycholate, 0.5% N-Lauroylsarcosine]. Chromatin was then sonicated for 20 cycles (30 s on, 45 s off) using Bioruptor (Diagenode, Seraing, Belgium). After sonication, the material was centrifuged at 16 000 g during 3 min at 4°C, with the supernatant representing the sonicated chromatin. About 75 µl was not subject to immunoprecipitation, thus representing total input control for the ChIP reactions. A total of 750 µl was incubated with 10 µg of anti-H3K9me3 antibody (Abcam, #8898, reported suitable for ChIP) overnight at 4°C. On day 2, magnetic Dynabeads G (Thermo Fisher Scientific) at 10× volume of H3K9me3 antibody were aliquoted into a new microtube. Magnetic beads were washed five times with cold RIPA wash buffer (50 mM Hepes, 500 mM LiCl, 1 mM EDTA, 1% NP-40, 0.7% Na-Deoxycholate). Next, beads were washed once with 1 ml TE + 50 mM NaCl on ice and sample was centrifuged at 950 g for 3 min at 4°C. After removing all liquid from beads, elution buffer (50 mM Tris, 10 mM EDTA, 1% SDS) was added for 15 min at 65°C. Finally, beads were centrifuged for 1 min at 1600 g and placed on a magnetholder to settle and the supernatant was transferred into a new tube. To reverse crosslinking, 3× volume of the elution buffer was added to the input and left to incubate together with the ChIP sample at 65°C overnight. On day 3, 1× volume of TE buffer and 0.2 mg ml^{-1} RNase were added and incubated for 1 h at 37°C. Afterwards, 0.2 mg ml^{-1} Proteinase K was added and incubated for 2 h at 55°C to digest proteins. Next, DNA was phenol-chloroform extracted at room temperature with 1× volume of 25:24:1 phenol-chloroform-isoamyl alcohol and centrifuged for 5 min to separate layers, followed by the addition of 1× volume chloroform. The DNA was then transferred to a new tube for precipitation with 1/10 of NaOAc 3 M, 1 µl 20 mg ml^{-1} glycogen, 2× volume of ice cold ethanol during 30 min at −80°C. After a centrifugation during 30 min at 4°C, the supernatant was removed and we added 0.5 ml ice cold 70% ethanol followed by 5 min centrifugation. After removing the ethanol, the pellet was air-dried at room temperature and resuspended in 40 µl dH_2O.

ChIP-seq libraries from ChIP and input DNAs were prepared as described before (114). Libraries from H9 hESCs and NPCs were sequenced with a 2 × 75 bp read length on Illumina HiSeq4000 and HiSeq3000, respectively. For ChIP-seq, two biological replicates from independent experiments were analysed by using QuickNGS (Next-Generation Sequencing) pipeline (115). Quality check of sequencing data was performed with FastQC version 0.10.1 (Babraham Bioinformatics, Cambridge, UK). ChIP-seq sequencing reads were mapped with Burrows–Wheeler Aligner (116) to the Homo sapiens genome (Ensembl database version 87). For peak calling, the resulting Binary Alignment/Map files were analsed with MACS2 version 2.0.10 (117). The results comprise lists of significant peaks compared with the respective input DNA controls. QuickNGS pipeline identifies all genes which are 2000 bp up- or downstream from the MACS2 peaks. To identify differential read-enriched peak regions from ChIP-seq data between different conditions, we used bdgdiff module of MACS2. Data were uploaded into MySQL database. QuickNGS also provides password-protected track hubs for the UCSC Genome Browser with direct hyperlinks for visualization. For the analysis of the distribution of H3K9me3 peaks, regions were annotated using HOMER tool (118) and default parameters except ENSMEBL GTF file version release 81.

RNA seq

Total RNA was extracted using RNAbee (Tel-Test Inc., Friendswood, TX, USA). Libraries were prepared using the TruSeq Stranded mRNA Library Prep Kit. Library preparation started with 1 µg total RNA. After selection (using poly-T oligo-attached magnetic beads), mRNA was purified and fragmented using divalent cations under elevated temperature. The RNA fragments underwent reverse transcription using random primers followed by second strand complementary DNA (cDNA) synthesis with DNA Polymerase I and RNase H. After end repair and A-tailing, indexing adapters were ligated. The products were then purified and amplified (20 µl template, 14 PCR cycles) to create the final cDNA libraries. After library validation and quantification (Agilent 2100 Bioanalyzer), equimolar amounts of library were pooled. The pool was quantified by using the Peqlab KAPA Library Quantification Kit and the Applied Biosystems 7900HT Sequence Detection System. The pool was sequenced on an Illumina HiSeq 4000 sequencer with a paired-end (2 × 75 bp) protocol.

RNA-seq data were analysed using a QuickNGS pipeline (115). Basic read quality check was performed using FastQC and read statistics were obtained with SAMtools. The basic data processing consists of a splicing-aware alignment using Tophat2 (119) followed by reference-guided transcriptome reassembly with Cufflinks2 (120,121). Read count means, FC and *P*-values were calculated with DEseq2 (122) and gene expression for the individual samples was calculated with Cufflinks2 (120,121) as FPKMs, using in both cases genomic annotation from the Ensembl database version 87.

Western blot

Cells were scraped from tissue culture plates and lysed in protein cell lysis buffer [10 mM Tris–HCl, pH 7.4, 150 mM NaCl, 10 mM EDTA, 50 mM NaF, 1% Triton X-100, 0.1% SDS supplemented with 20 µg ml^{-1} Aprotinin, 2 mM sodium orthovanadate, 1 mM phenylmethylsulphonyl fluoride and protease inhibitor (Roche)] by incubating samples for 10 min on ice and homogenization through 27G syringe needle. Then, cell lysates were centrifuged at 10 000 *g* for 10 min at 4°C and the supernatant was collected. Protein concentrations were determined with a standard BCA protein assay (Thermo Fisher Scientific). Total protein was separated by SDS–PAGE, transferred to nitrocellulose membranes (Millipore,

Darmstadt, Germany) and subjected to immunoblotting. Western blot analysis was performed with anti-total HTT (Cell Signaling, #5656, 1:1,000), anti-polyQ-expanded HTT (DSHB, MW1, 1:500), anti-ATF7IP (Proteintech, 14699-1-AP, 1:500), anti-SETDB1 (Abcam, #107225, 1:500), anti-H3K9me3 (Abcam, #8898, 1:1,000), anti-H3 (Cell Signaling, #2650, 1:10,000), anti-OCT4 (Stem Cell Technologies, #60093, 1:500), anti-SOX2 (Abcam, #97959, 1:1,000), anti-PAX6 (Stem Cell Technologies, #60094, 1:200) and anti-ß-actin (Abcam, #8226, 1:1,000).

Immunocytochemistry

Cells were fixed with paraformaldehyde (4% in PBS) for 30 min, followed by permeabilization (0.2% Triton X-100 in PBS for 10 min) and blocking (3% BSA in 0.2% Triton X-100 in PBS for 10 min). Cells were incubated in primary antibody for 2 h at room temperature [Mouse anti-SETDB1 (Abcam, #107225, 1:200), Rabbit anti-ATF7IP (Proteintech, #14699-1-AP, 1:500), Rabbit anti-H3K9me3 (Abcam, #8898, 1:500), Mouse anti-OCT4 (Stem Cell Technologies, #60093, 1:200), Rabbit anti-PAX6 (Stem Cell Technologies, #60094, 1:300), Mouse anti-MAP2 (Sigma, #1406, 1:200), Mouse anti-polyQ (Millipore, MAB1574, 1:50)]. Then, cells were washed with 0.2% Triton-X/PBS and incubated with secondary antibody [Alexa Fluor 488 goat anti-mouse (Thermo Fisher Scientific, A-11029, 1:500); Alexa Fluor 568 goat anti-rabbit (Thermo Fisher Scientific, A-11011, 1:500) and 2 µg ml^{-1} Hoechst 33342 (Life Technologies, #1656104)] for 1 h at room temperature. About 0.2% Triton-X/PBS and distilled water wash were followed before the cover slips were mounted.

RNA isolation and real-time qPCR

Total RNA was extracted using RNAbee (Tel-Test Inc.). cDNA was generated using qScript Flex cDNA synthesis kit (Quantabio, Beverly, MA, USA). SybrGreen real-time qPCR experiments were performed with a 1:20 dilution of cDNA using a CFC384 Real-Time System (Bio-Rad) following the manufacturer's instructions. Data were analysed with the comparative $2\Delta\Delta C_t$ method using the geometric mean of *ACTB* and *GAPDH* as housekeeping genes. See Supplementary Table S3 for details about the primers used for this assay.

Statistical analysis

Statistical comparisons of qPCR data and SETDB1 levels in co-IP experiments followed by western blot were performed with Student's *t*-test for unpaired samples using GraphPad Prism 6.0. Significant differences from proteomics data were determined with Perseus (v. 1.5.2.4) (111) after correction for multiple testing following the Benjamini–Hochberg procedure, which calculates false discovery rate (FDR) adjusted *P*-values. Analysis of enriched GOBPs were performed using Database for Annotation Visualization and Integrated Discovery (123), which provides statistical comparisons with a modified Fisher's exact test (EASE score). We used MACS2 to calculate FC and *P*-values from ChIP-seq data, allowing for the identification of significant differential enriched-peak regions between distinct conditions (117). For RNA-seq data, FC and *P*-values were calculated with DEseq2 (122) and gene expression for the individual samples was calculated with Cufflinks2 (120,121) as FPKMs.

Data availability

The accession number for the ChIP-seq and RNA-seq datasets reported in this paper is GEO: GSE118325.

Supplementary Materials

Supplementary Materials are available at *HMG* online.

Funding

European Commission (FP7-PEOPLE-2013-CIG) and the Else Kröner-Fresenius-Stiftung (2015_A118).

Conflict of Interest statement. None declared.

References

1. Finkbeiner, S. (2011) Huntington's disease. *Cold Spring Harb. Perspect. Biol.*, **3**, 1–24.
2. Koyuncu, S., Fatima, A., Gutierrez-Garcia, R. and Vilchez, D. (2017) Proteostasis of huntingtin in health and disease. *Int. J. Mol. Sci.*, **18,** 1–18.
3. Cattaneo, E., Zuccato, C. and Tartari, M. (2005) Normal huntingtin function: an alternative approach to Huntington's disease. *Nat. Rev. Neurosci.*, **6**, 919–930.
4. Saudou, F. and Humbert, S. (2016) The biology of huntingtin. *Neuron*, **89**, 910–926.
5. Vonsattel, J.P., Keller, C. and Del Pilar Amaya, M. (2008) Neuropathology of Huntington's disease. *Handb. Clin. Neurol.*, **89**, 599–618.
6. Dragatsis, I., Levine, M.S. and Zeitlin, S. (2000) Inactivation of Hdh in the brain and testis results in progressive neurodegeneration and sterility in mice. *Nat. Genet.*, **26**, 300–306.
7. Gauthier, L.R., Charrin, B.C., Borrell-Pages, M., Dompierre, J.P., Rangone, H., Cordelieres, F.P., De Mey, J., MacDonald, M.E., Lessmann, V., Humbert, S. *et al.* (2004) Huntingtin controls neurotrophic support and survival of neurons by enhancing BDNF vesicular transport along microtubules. *Cell*, **118**, 127–138.
8. Gunawardena, S., Her, L.S., Brusch, R.G., Laymon, R.A., Niesman, I.R., Gordesky-Gold, B., Sintasath, L., Bonini, N.M. and Goldstein, L.S. (2003) Disruption of axonal transport by loss of huntingtin or expression of pathogenic polyQ proteins in Drosophila. *Neuron*, **40**, 25–40.
9. O'Kusky, J.R., Nasir, J., Cicchetti, F., Parent, A. and Hayden, M.R. (1999) Neuronal degeneration in the basal ganglia and loss of pallido-subthalamic synapses in mice with targeted disruption of the Huntington's disease gene. *Brain Res.*, **818**, 468–479.
10. Trushina, E., Dyer, R.B., Badger, J.D. 2nd, Ure, D., Eide, L., Tran, D.D., Vrieze, B.T., Legendre-Guillemin, V., McPherson, P.S., Mandavilli, B.S. *et al.* (2004) Mutant huntingtin impairs axonal trafficking in mammalian neurons in vivo and in vitro. *Mol. Cell. Biol.*, **24**, 8195–8209.
11. Ho, L.W., Brown, R., Maxwell, M., Wyttenbach, A. and Rubinsztein, D.C. (2001) Wild-type huntingtin reduces the cellular toxicity of mutant huntingtin in mammalian cell models of Huntington's disease. *J. Med. Genet.*, **38**, 450–452.
12. Leavitt, B.R., Guttman, J.A., Hodgson, J.G., Kimel, G.H., Singaraja, R., Vogl, A.W. and Hayden, M.R. (2001) Wild-type huntingtin reduces the cellular toxicity of mutant huntingtin in vivo. *Am. J. Hum. Genet.*, **68**, 313–324.
13. Leavitt, B.R., van Raamsdonk, J.M., Shehadeh, J., Fernandes, H., Murphy, Z., Graham, R.K., Wellington, C.L., Raymond, L.A. and Hayden, M.R. (2006) Wild-type huntingtin protects neurons from excitotoxicity. *J. Neurochem.*, **96**, 1121–1129.
14. Rigamonti, D., Bauer, J.H., De-Fraja, C., Conti, L., Sipione, S., Sciorati, C., Clementi, E., Hackam, A., Hayden, M.R.,

Li, Y. *et al.* (2000) Wild-type huntingtin protects from apoptosis upstream of caspase-3. *J. Neurosci.*, **20**, 3705–3713.
15. Sun, Y., Savanenin, A., Reddy, P.H. and Liu, Y.F. (2001) Polyglutamine-expanded huntingtin promotes sensitization of N-methyl-D-aspartate receptors via post-synaptic density 95. *J. Biol. Chem.*, **276**, 24713–24718.
16. Zuccato, C., Ciammola, A., Rigamonti, D., Leavitt, B.R., Goffredo, D., Conti, L., MacDonald, M.E., Friedlander, R.M., Silani, V., Hayden, M.R. *et al.* (2001) Loss of huntingtin-mediated BDNF gene transcription in Huntington's disease. *Science*, **293**, 493–498.
17. Zuccato, C., Tartari, M., Crotti, A., Goffredo, D., Valenza, M., Conti, L., Cataudella, T., Leavitt, B.R., Hayden, M.R., Timmusk, T. *et al.* (2003) Huntingtin interacts with REST/NRSF to modulate the transcription of NRSE-controlled neuronal genes. *Nat. Genet.*, **35**, 76–83.
18. Duyao, M.P., Auerbach, A.B., Ryan, A., Persichetti, F., Barnes, G.T., McNeil, S.M., Ge, P., Vonsattel, J.P., Gusella, J.F., Joyner, A.L. *et al.* (1995) Inactivation of the mouse Huntington's disease gene homolog Hdh. *Science*, **269**, 407–410.
19. Nasir, J., Floresco, S.B., O'Kusky, J.R., Diewert, V.M., Richman, J.M., Zeisler, J., Borowski, A., Marth, J.D., Phillips, A.G. and Hayden, M.R. (1995) Targeted disruption of the Huntington's disease gene results in embryonic lethality and behavioral and morphological changes in heterozygotes. *Cell*, **81**, 811–823.
20. Zeitlin, S., Liu, J.P., Chapman, D.L., Papaioannou, V.E. and Efstratiadis, A. (1995) Increased apoptosis and early embryonic lethality in mice nullizygous for the Huntington's disease gene homologue. *Nat. Genet.*, **11**, 155–163.
21. White, J.K., Auerbach, W., Duyao, M.P., Vonsattel, J.P., Gusella, J.F., Joyner, A.L. and MacDonald, M.E. (1997) Huntingtin is required for neurogenesis and is not impaired by the Huntington's disease CAG expansion. *Nat. Genet.*, **17**, 404–410.
22. Godin, J.D., Colombo, K., Molina-Calavita, M., Keryer, G., Zala, D., Charrin, B.C., Dietrich, P., Volvert, M.L., Guillemot, F., Dragatsis, I. *et al.* (2010) Huntingtin is required for mitotic spindle orientation and mammalian neurogenesis. *Neuron*, **67**, 392–406.
23. Conforti, P., Camnasio, S., Mutti, C., Valenza, M., Thompson, M., Fossale, E., Zeitlin, S., MacDonald, M.E., Zuccato, C. and Cattaneo, E. (2013) Lack of huntingtin promotes neural stem cells differentiation into glial cells while neurons expressing huntingtin with expanded polyglutamine tracts undergo cell death. *Neurobiol. Dis.*, **50**, 160–170.
24. Nguyen, G.D., Gokhan, S., Molero, A.E. and Mehler, M.F. (2013) Selective roles of normal and mutant huntingtin in neural induction and early neurogenesis. *PLoS One*, **8**, e64368.
25. Myers, R.H., Leavitt, J., Farrer, L.A., Jagadeesh, J., McFarlane, H., Mastromauro, C.A., Mark, R.J. and Gusella, J.F. (1989) Homozygote for Huntington disease. *Am. J. Hum. Genet.*, **45**, 615–618.
26. Wexler, N.S., Young, A.B., Tanzi, R.E., Travers, H., Starosta-Rubinstein, S., Penney, J.B., Snodgrass, S.R., Shoulson, I., Gomez, F., Ramos Arroyo, M.A. *et al.* (1987) Homozygotes for Huntington's disease. *Nature*, **326**, 194–197.
27. Batista, C.M., Kippin, T.E., Willaime-Morawek, S., Shimabukuro, M.K., Akamatsu, W. and van der Kooy, D. (2006) A progressive and cell non-autonomous increase in striatal neural stem cells in the Huntington's disease R6/2 mouse. *J. Neurosci.*, **26**, 10452–10460.
28. Curtis, M.A., Penney, E.B., Pearson, A.G., van Roon-Mom, W.M., Butterworth, N.J., Dragunow, M., Connor, B. and Faull, R.L. (2003) Increased cell proliferation and neurogenesis in the adult human Huntington's disease brain. *Proc. Natl. Acad. Sci. U.S.A.*, **100**, 9023–9027.
29. Curtis, M.A., Penney, E.B., Pearson, J., Dragunow, M., Connor, B. and Faull, R.L. (2005) The distribution of progenitor cells in the subependymal layer of the lateral ventricle in the normal and Huntington's disease human brain. *Neuroscience*, **132**, 777–788.
30. Molero, A.E., Gokhan, S., Gonzalez, S., Feig, J.L., Alexandre, L.C. and Mehler, M.F. (2009) Impairment of developmental stem cell-mediated striatal neurogenesis and pluripotency genes in a knock-in model of Huntington's disease. *Proc. Natl. Acad. Sci. U.S.A.*, **106**, 21900–21905.
31. Brandt, J., Shpritz, B., Codori, A.M., Margolis, R. and Rosenblatt, A. (2002) Neuropsychological manifestations of the genetic mutation for Huntington's disease in presymptomatic individuals. *J. Int. Neuropsychol. Soc.*, **8**, 918–924.
32. Joshi, P.R., Wu, N.P., Andre, V.M., Cummings, D.M., Cepeda, C., Joyce, J.A., Carroll, J.B., Leavitt, B.R., Hayden, M.R., Levine, M.S. *et al.* (2009) Age-dependent alterations of corticostriatal activity in the YAC128 mouse model of Huntington disease. *J. Neurosci.*, **29**, 2414–2427.
33. Milnerwood, A.J. and Raymond, L.A. (2010) Early synaptic pathophysiology in neurodegeneration: insights from Huntington's disease. *Trends Neurosci.*, **33**, 513–523.
34. Murphy, K.P., Carter, R.J., Lione, L.A., Mangiarini, L., Mahal, A., Bates, G.P., Dunnett, S.B. and Morton, A.J. (2000) Abnormal synaptic plasticity and impaired spatial cognition in mice transgenic for exon 1 of the human Huntington's disease mutation. *J. Neurosci.*, **20**, 5115–5123.
35. Paulsen, J.S., Langbehn, D.R., Stout, J.C., Aylward, E., Ross, C.A., Nance, M., Guttman, M., Johnson, S., MacDonald, M., Beglinger, L.J. *et al.* (2008) Detection of Huntington's disease decades before diagnosis: the Predict-HD study. *J. Neurol. Neurosurg. Psychiatry*, **79**, 874–880.
36. Paulsen, J.S., Magnotta, V.A., Mikos, A.E., Paulson, H.L., Penziner, E., Andreasen, N.C. and Nopoulos, P.C. (2006) Brain structure in preclinical Huntington's disease. *Biol. Psychiatry*, **59**, 57–63.
37. Schippling, S., Schneider, S.A., Bhatia, K.P., Munchau, A., Rothwell, J.C., Tabrizi, S.J. and Orth, M. (2009) Abnormal motor cortex excitability in preclinical and very early Huntington's disease. *Biol. Psychiatry*, **65**, 959–965.
38. HD iPSC Consortium (2012) Induced pluripotent stem cells from patients with Huntington's disease show CAG-repeat-expansion-associated phenotypes. *Cell Stem Cell*, **11**, 264–278.
39. HD iPSC Consortium (2017) Developmental alterations in Huntington's disease neural cells and pharmacological rescue in cells and mice. *Nat. Neurosci.*, **20**, 648–660.
40. Valor, L.M. (2015) Transcription, epigenetics and ameliorative strategies in Huntington's disease: a genome-wide perspective. *Mol. Neurobiol.*, **51**, 406–423.
41. Achour, M., Le Gras, S., Keime, C., Parmentier, F., Lejeune, F.X., Boutillier, A.L., Neri, C., Davidson, I. and Merienne, K. (2015) Neuronal identity genes regulated by super-enhancers are preferentially down-regulated in the striatum of Huntington's disease mice. *Hum. Mol. Genet.*, **24**, 3481–3496.
42. Bai, G., Cheung, I., Shulha, H.P., Coelho, J.E., Li, P., Dong, X.J., Jakovcevski, M., Wang, Y.M., Grigorenko, A., Jiang, Y. *et al.* (2015) Epigenetic dysregulation of hairy and

enhancer of split 4 (HES4) is associated with striatal degeneration in postmortem Huntington brains. *Hum. Mol. Genet.*, **24**, 1441–1456.
43. Francelle, L., Lotz, C., Outeiro, T., Brouillet, E. and Merienne, K. (2017) Contribution of neuroepigenetics to Huntington's disease. *Front. Hum. Neurosci.*, **11**, 17.
44. Glajch, K.E. and Sadri-Vakili, G. (2015) Epigenetic mechanisms involved in Huntington's disease pathogenesis. *J. Huntingtons Dis.*, **4**, 1–15.
45. McFarland, K.N., Das, S., Sun, T.T., Leyfer, D., Xia, E., Sangrey, G.R., Kuhn, A., Luthi-Carter, R., Clark, T.W., Sadri-Vakili, G. *et al.* (2012) Genome-wide histone acetylation is altered in a transgenic mouse model of Huntington's disease. *Plos One*, **7** ,e41423.
46. Sadri-Vakili, G., Bouzou, B., Benn, C.L., Kim, M.O., Chawla, P., Overland, R.P., Glajch, K.E., Xia, E., Qiu, Z., Hersch, S.M. *et al.* (2007) Histones associated with downregulated genes are hypo-acetylated in Huntington's disease models. *Hum. Mol. Genet.*, **16**, 1293–1306.
47. Valor, L.M., Guiretti, D., Lopez-Atalaya, J.P. and Barco, A. (2013) Genomic landscape of transcriptional and epigenetic dysregulation in early onset polyglutamine disease. *J. Neurosci.*, **33**, 10471–10482.
48. Vashishtha, M., Ng, C.W., Yildirim, F., Gipson, T.A., Kratter, I.H., Bodai, L., Song, W., Lau, A., Labadorf, A., Vogel-Ciernia, A. *et al.* (2013) Targeting H3K4 trimethylation in Huntington disease. *Proc. Natl. Acad. Sci. U.S.A.*, **110**, E3027–E3036.
49. Biagioli, M., Ferrari, F., Mendenhall, E.M., Zhang, Y., Erdin, S., Vijayvargia, R., Vallabh, S.M., Solomos, N., Manavalan, P., Ragavendran, A. *et al.* (2015) Htt CAG repeat expansion confers pleiotropic gains of mutant huntingtin function in chromatin regulation. *Hum. Mol. Genet.*, **24**, 2442–2457.
50. Xia, J., Lee, D.H., Taylor, J., Vandelft, M. and Truant, R. (2003) Huntingtin contains a highly conserved nuclear export signal. *Hum. Mol. Genet.*, **12**, 1393–1403.
51. Cornett, J., Cao, F., Wang, C.E., Ross, C.A., Bates, G.P., Li, S.H. and Li, X.J. (2005) Polyglutamine expansion of huntingtin impairs its nuclear export. *Nat. Genet.*, **37**, 198–204.
52. Ferrante, R.J., Ryu, H., Kubilus, J.K., D'Mello, S., Sugars, K.L., Lee, J., Lu, P., Smith, K., Browne, S., Beal, M.F. *et al.* (2004) Chemotherapy for the brain: the antitumor antibiotic mithramycin prolongs survival in a mouse model of Huntington's disease. *J. Neurosci.*, **24**, 10335–10342.
53. Gardian, G., Browne, S.E., Choi, D.K., Klivenyi, P., Gregorio, J., Kubilus, J.K., Ryu, H., Langley, B., Ratan, R.R., Ferrante, R.J. *et al.* (2005) Neuroprotective effects of phenylbutyrate in the N171-82Q transgenic mouse model of Huntington's disease. *J. Biol. Chem.*, **280**, 556–563.
54. Ryu, H., Lee, J., Hagerty, S.W., Soh, B.Y., McAlpin, S.E., Cormier, K.A., Smith, K.M. and Ferrante, R.J. (2006) ESET/SETDB1 gene expression and histone H3 (K9) trimethylation in Huntington's disease. *Proc. Natl. Acad. Sci. U.S.A.*, **103**, 19176–19181.
55. Stack, E.C., Del Signore, S.J., Luthi-Carter, R., Soh, B.Y., Goldstein, D.R., Matson, S., Goodrich, S., Markey, A.L., Cormier, K., Hagerty, S.W. *et al.* (2007) Modulation of nucleosome dynamics in Huntington's disease. *Hum. Mol. Genet.*, **16**, 1164–1175.
56. Becker, J.S., Nicetto, D. and Zaret, K.S. (2016) H3K9me3-dependent heterochromatin: barrier to cell fate changes. *Trends Genet.*, **32**, 29–41.
57. Hawkins, R.D., Hon, G.C., Lee, L.K., Ngo, Q., Lister, R., Pelizzola, M., Edsall, L.E., Kuan, S., Luu, Y., Klugman, S. *et al.* (2010) Distinct epigenomic landscapes of pluripotent and lineage-committed human cells. *Cell Stem Cell*, **6**, 479–491.
58. Meshorer, E. and Misteli, T. (2006) Chromatin in pluripotent embryonic stem cells and differentiation. *Nat. Rev. Mol. Cell Biol.*, **7**, 540–546.
59. Fujita, N., Watanabe, S., Ichimura, T., Ohkuma, Y., Chiba, T., Saya, H. and Nakao, M. (2003) MCAF mediates MBD1-dependent transcriptional repression. *Mol. Cell. Biol.*, **23**, 2834–2843.
60. Wang, H., An, W., Cao, R., Xia, L., Erdjument-Bromage, H., Chatton, B., Tempst, P., Roeder, R.G. and Zhang, Y. (2003) mAM facilitates conversion by ESET of dimethyl to trimethyl lysine 9 of histone H3 to cause transcriptional repression. *Mol. Cell*, **12**, 475–487.
61. Peters, M.F. and Ross, C.A. (2001) Isolation of a 40-kDa huntingtin-associated protein. *J. Biol. Chem.*, **276**, 3188–3194.
62. Fujita, K., Nakamura, Y., Oka, T., Ito, H., Tamura, T., Tagawa, K., Sasabe, T., Katsuta, A., Motoki, K., Shiwaku, H. *et al.* (2013) A functional deficiency of TERA/VCP/p97 contributes to impaired DNA repair in multiple polyglutamine diseases. *Nat. Commun.*, **4**, 1816.
63. Ichimura, T., Watanabe, S., Sakamoto, Y., Aoto, T., Fujita, N. and Nakao, M. (2005) Transcriptional repression and heterochromatin formation by MBD1 and MCAF/AM family proteins. *J. Biol. Chem.*, **280**, 13928–13935.
64. Minkovsky, A., Sahakyan, A., Rankin-Gee, E., Bonora, G., Patel, S. and Plath, K. (2014) The Mbd1-Atf7ip-Setdb1 pathway contributes to the maintenance of X chromosome inactivation. *Epigenetics Chromatin*, **7**, 12.
65. Timms, R.T., Tchasovnikarova, I.A., Antrobus, R., Dougan, G. and Lehner, P.J. (2016) ATF7IP-mediated stabilization of the histone methyltransferase SETDB1 is essential for heterochromatin formation by the HUSH complex. *Cell Rep.*, **17**, 653–659.
66. Chuang, J.H., Tung, L.C. and Lin, Y. (2015) Neural differentiation from embryonic stem cells in vitro: an overview of the signaling pathways. *World J. Stem Cells*, **7**, 437–447.
67. Callaerts, P., Halder, G. and Gehring, W.J. (1997) PAX-6 in development and evolution. *Annu. Rev. Neurosci.*, **20**, 483–532.
68. Liao, J., Karnik, R., Gu, H., Ziller, M.J., Clement, K., Tsankov, A.M., Akopian, V., Gifford, C.A., Donaghey, J., Galonska, C. *et al.* (2015) Targeted disruption of DNMT1, DNMT3A and DNMT3B in human embryonic stem cells. *Nat. Genet.*, **47**, 469–478.
69. Zhang, X., Li, B., Li, W., Ma, L., Zheng, D., Li, L., Yang, W., Chu, M., Chen, W., Mailman, R.B. *et al.* (2014) Transcriptional repression by the BRG1-SWI/SNF complex affects the pluripotency of human embryonic stem cells. *Stem Cell Reports*, **3**, 460–474.
70. Rowbotham, S.P., Barki, L., Neves-Costa, A., Santos, F., Dean, W., Hawkes, N., Choudhary, P., Will, W.R., Webster, J., Oxley, D. *et al.* (2011) Maintenance of silent chromatin through replication requires SWI/SNF-like chromatin remodeler SMARCAD1. *Mol. Cell*, **42**, 285–296.
71. Dutta, B., Ren, Y., Hao, P., Sim, K.H., Cheow, E., Adav, S., Tam, J.P. and Sze, S.K. (2014) Profiling of the chromatin-associated proteome identifies HP1BP3 as a novel regulator of cell cycle progression. *Mol. Cell. Proteomics*, **13**, 2183–2197.
72. Dutta, B., Yan, R., Lim, S.K., Tam, J.P. and Sze, S.K. (2014) Quantitative profiling of chromatome dynamics reveals a novel role for HP1BP3 in hypoxia-induced oncogenesis. *Mol. Cell. Proteomics*, **13**, 3236–3249.

73. Ozturk, N., Singh, I., Mehta, A., Braun, T. and Barreto, G. (2014) HMGA proteins as modulators of chromatin structure during transcriptional activation. *Front. Cell Dev. Biol.*, **2**, 5.
74. Lee, J.H. and Skalnik, D.G. (2008) Wdr82 is a C-terminal domain-binding protein that recruits the Setd1A histone H3-Lys4 methyltransferase complex to transcription start sites of transcribed human genes. *Mol. Cell. Biol.*, **28**, 609–618.
75. Chan, C.W., Lee, Y.B., Uney, J., Flynn, A., Tobias, J.H. and Norman, M. (2007) A novel member of the SAF (scaffold attachment factor)-box protein family inhibits gene expression and induces apoptosis. *Biochem. J.*, **407**, 355–362.
76. Brackertz, M., Boeke, J., Zhang, R. and Renkawitz, R. (2002) Two highly related p66 proteins comprise a new family of potent transcriptional repressors interacting with MBD2 and MBD3. *J. Biol. Chem.*, **277**, 40958–40966.
77. Rodriguez, P., Munroe, D., Prawitt, D., Chu, L.L., Bric, E., Kim, J., Reid, L.H., Davies, C., Nakagama, H., Loebbert, R. *et al.* (1997) Functional characterization of human nucleosome assembly protein-2 (NAP1L4) suggests a role as a histone chaperone. *Genomics*, **44**, 253–265.
78. Gallant, P. (2007) Control of transcription by pontin and reptin. *Trends Cell Biol.*, **17**, 187–192.
79. Maertens, G.N., El Messaoudi-Aubert, S., Elderkin, S., Hiom, K. and Peters, G. (2010) Ubiquitin-specific proteases 7 and 11 modulate polycomb regulation of the INK4a tumour suppressor. *EMBO J.*, **29**, 2553–2565.
80. Morey, L., Santanach, A., Blanco, E., Aloia, L., Nora, E.P., Bruneau, B.G. and Di Croce, L. (2015) Polycomb regulates mesoderm cell fate-specification in embryonic stem cells through activation and repression mechanisms. *Cell Stem Cell*, **17**, 300–315.
81. Yao, M., Zhou, X., Zhou, J., Gong, S., Hu, G., Li, J., Huang, K., Lai, P., Shi, G., Hutchins, A.P. *et al.* (2018) PCGF5 is required for neural differentiation of embryonic stem cells. *Nat. Commun.*, **9**, 1463.
82. Peters, A.H., Kubicek, S., Mechtler, K., O'Sullivan, R.J., Derijck, A.A., Perez-Burgos, L., Kohlmaier, A., Opravil, S., Tachibana, M., Shinkai, Y. *et al.* (2003) Partitioning and plasticity of repressive histone methylation states in mammalian chromatin. *Mol. Cell*, **12**, 1577–1589.
83. Rea, S., Eisenhaber, F., O'Carroll, D., Strahl, B.D., Sun, Z.W., Schmid, M., Opravil, S., Mechtler, K., Ponting, C.P., Allis, C.D. *et al.* (2000) Regulation of chromatin structure by site-specific histone H3 methyltransferases. *Nature*, **406**, 593–599.
84. Fritsch, L., Robin, P., Mathieu, J.R., Souidi, M., Hinaux, H., Rougeulle, C., Harel-Bellan, A., Ameyar-Zazoua, M. and Ait-Si-Ali, S. (2010) A subset of the histone H3 lysine 9 methyltransferases Suv39h1, G9a, GLP, and SETDB1 participate in a multimeric complex. *Mol. Cell*, **37**, 46–56.
85. Radoja, N., Guerrini, L., Lo Iacono, N., Merlo, G.R., Costanzo, A., Weinberg, W.C., La Mantia, G., Calabro, V. and Morasso, M.I. (2007) Homeobox gene Dlx3 is regulated by p63 during ectoderm development: relevance in the pathogenesis of ectodermal dysplasias. *Development*, **134**, 13–18.
86. Ziller, M.J., Edri, R., Yaffe, Y., Donaghey, J., Pop, R., Mallard, W., Issner, R., Gifford, C.A., Goren, A., Xing, J. *et al.* (2015) Dissecting neural differentiation regulatory networks through epigenetic footprinting. *Nature*, **518**, 355–359.
87. Rhinn, M., Lun, K., Ahrendt, R., Geffarth, M. and Brand, M. (2009) Zebrafish gbx1 refines the midbrain-hindbrain boundary border and mediates the Wnt8 posteriorization signal. *Neural Dev.*, **4**, 12.
88. Bestman, J.E. and Cline, H.T. (2008) The RNA binding protein CPEB regulates dendrite morphogenesis and neuronal circuit assembly in vivo. *Proc. Natl. Acad. Sci. U.S.A.*, **105**, 20494–20499.
89. Bezprozvanny, I. and Hayden, M.R. (2004) Deranged neuronal calcium signaling and Huntington disease. *Biochem. Biophys. Res. Commun.*, **322**, 1310–1317.
90. Nair, A.G., Bhalla, U.S. and Hellgren Kotaleski, J. (2016) Role of DARPP-32 and ARPP-21 in the emergence of temporal constraints on striatal calcium and dopamine integration. *PLoS Comput. Biol.*, **12**, e1005080.
91. Bardoni, R., Tawfik, V.L., Wang, D., Francois, A., Solorzano, C., Shuster, S.A., Choudhury, P., Betelli, C., Cassidy, C., Smith, K. *et al.* (2014) Delta opioid receptors presynaptically regulate cutaneous mechanosensory neuron input to the spinal cord dorsal horn. *Neuron*, **81**, 1312–1327.
92. Park, I.H., Arora, N., Huo, H., Maherali, N., Ahfeldt, T., Shimamura, A., Lensch, M.W., Cowan, C., Hochedlinger, K. and Daley, G.Q. (2008) Disease-specific induced pluripotent stem cells. *Cell*, **134**, 877–886.
93. Noormohammadi, A., Khodakarami, A., Gutierrez-Garcia, R., Lee, H.J., Koyuncu, S., Konig, T., Schindler, C., Saez, I., Fatima, A., Dieterich, C. *et al.* (2016) Somatic increase of CCT8 mimics proteostasis of human pluripotent stem cells and extends C. elegans lifespan. *Nat. Commun.*, **7**, 13649.
94. Trottier, Y., Lutz, Y., Stevanin, G., Imbert, G., Devys, D., Cancel, G., Saudou, F., Weber, C., David, G., Tora, L. *et al.* (1995) Polyglutamine expansion as a pathological epitope in Huntington's disease and four dominant cerebellar ataxias. *Nature*, **378**, 403–406.
95. Jeon, I., Lee, N., Li, J.Y., Park, I.H., Park, K.S., Moon, J., Shim, S.H., Choi, C., Chang, D.J., Kwon, J. *et al.* (2012) Neuronal properties, in vivo effects, and pathology of a Huntington's disease patient-derived induced pluripotent stem cells. *Stem Cells*, **30**, 2054–2062.
96. Koyuncu, S., Saez, I., Lee, H.J., Gutierrez-Garcia, R., Pokrzywa, W., Fatima, A., Hoppe, T. and Vilchez, D. (2018) The ubiquitin ligase UBR5 suppresses proteostasis collapse in pluripotent stem cells from Huntington's disease patients. *Nat. Commun.*, **9**, 2886.
97. Noormohammadi, A., Calculli, G., Gutierrez-Garcia, R., Khodakarami, A., Koyuncu, S. and Vilchez, D. (2018) Mechanisms of protein homeostasis (proteostasis) maintain stem cell identity in mammalian pluripotent stem cells. *Cell. Mol. Life Sci.* **75**, 275–290.
98. DiFiglia, M., Sapp, E., Chase, K., Schwarz, C., Meloni, A., Young, C., Martin, E., Vonsattel, J.P., Carraway, R., Reeves, S.A. *et al.* (1995) Huntingtin is a cytoplasmic protein associated with vesicles in human and rat brain neurons. *Neuron*, **14**, 1075–1081.
99. Hoffner, G., Kahlem, P. and Djian, P. (2002) Perinuclear localization of huntingtin as a consequence of its binding to microtubules through an interaction with beta-tubulin: relevance to Huntington's disease. *J. Cell Sci.*, **115**, 941–948.
100. Velier, J., Kim, M., Schwarz, C., Kim, T.W., Sapp, E., Chase, K., Aronin, N. and DiFiglia, M. (1998) Wild-type and mutant huntingtins function in vesicle trafficking in the secretory and endocytic pathways. *Exp. Neurol.*, **152**, 34–40.

101. Rui, Y.N., Xu, Z., Patel, B., Chen, Z., Chen, D., Tito, A., David, G., Sun, Y., Stimming, E.F., Bellen, H.J. *et al.* (2015) Huntingtin functions as a scaffold for selective macroautophagy. *Nat. Cell Biol.*, **17**, 262–275.
102. Seong, I.S., Woda, J.M., Song, J.J., Lloret, A., Abeyrathne, P.D., Woo, C.J., Gregory, G., Lee, J.M., Wheeler, V.C., Walz, T. *et al.* (2010) Huntingtin facilitates polycomb repressive complex 2. *Hum. Mol. Genet.*, **19**, 573–583.
103. Di Croce, L. and Helin, K. (2013) Transcriptional regulation by polycomb group proteins. *Nat. Struct. Mol. Biol.*, **20**, 1147–1155.
104. Tousley, A. and Kegel-Gleason, K.B. (2016) Induced pluripotent stem cells in Huntington's disease research: progress and opportunity. *J. Huntingtons Dis.*, **5**, 99–131.
105. Valcarcel-Ocete, L., Alkorta-Aranburu, G., Iriondo, M., Fullaondo, A., Garcia-Barcina, M., Fernandez-Garcia, J.M., Lezcano-Garcia, E., Losada-Domingo, J.M., Ruiz-Ojeda, J., Alvarez de Arcaya, A. *et al.* (2015) Exploring genetic factors involved in Huntington disease age of onset: E2F2 as a new potential modifier gene. *PLoS One*, **10**, e0131573.
106. Chambers, S.M., Fasano, C.A., Papapetrou, E.P., Tomishima, M., Sadelain, M. and Studer, L. (2009) Highly efficient neural conversion of human ES and iPS cells by dual inhibition of SMAD signaling. *Nat. Biotechnol.*, **27**, 275–280.
107. Vilchez, D., Boyer, L., Morantte, I., Lutz, M., Merkwirth, C., Joyce, D., Spencer, B., Page, L., Masliah, E., Berggren, T.W. *et al.* (2012) Increased proteasome activity in human embryonic stem cells is regulated by PSMD11. *Nature*, **489**, 304–308.
108. Lee, H.J., Bartsch, D., Xiao, C., Guerrero, S., Ahuja, G., Schindler, C., Moresco, J.J., Yates, J.R. 3rd, Gebauer, F., Bazzi, H. *et al.* (2017) A post-transcriptional program coordinated by CSDE1 prevents intrinsic neural differentiation of human embryonic stem cells. *Nat. Commun.*, **8**, 1456.
109. Rappsilber, J., Ishihama, Y. and Mann, M. (2003) Stop and go extraction tips for matrix-assisted laser desorption/ionization, nanoelectrospray, and LC/MS sample pretreatment in proteomics. *Anal. Chem.*, **75**, 663–670.
110. Cox, J., Hein, M.Y., Luber, C.A., Paron, I., Nagaraj, N. and Mann, M. (2014) Accurate proteome-wide label-free quantification by delayed normalization and maximal peptide ratio extraction, termed MaxLFQ. *Mol. Cell. Proteomics*, **13**, 2513–2526.
111. Cox, J. and Mann, M. (2012) 1D and 2D annotation enrichment: a statistical method integrating quantitative proteomics with complementary high-throughput data. *BMC Bioinformatics*, **13 (**Suppl 16**)**, S12.
112. Arrigoni, L., Al-Hasani, H., Ramirez, F., Panzeri, I., Ryan, D.P., Santacruz, D., Kress, N., Pospisilik, A.J., Boenisch, U. and Manke, T. (2018) Ultra-parallel ChIP-seq by barcoding of intact nuclei. *bioRxiv*, https://doi.org/10.1101/276469.
113. Rada-Iglesias, A., Bajpai, R., Swigut, T., Brugmann, S.A., Flynn, R.A. and Wysocka, J. (2011) A unique chromatin signature uncovers early developmental enhancers in humans. *Nature*, **470**, 279–283.
114. Rehimi, R., Bartusel, M., Solinas, F., Altmuller, J. and Rada-Iglesias, A. (2017) Chromatin Immunoprecipitation (ChIP) Protocol for low-abundance embryonic samples. *J. Vis. Exp.*, **126**, e56186.
115. Wagle, P., Nikolic, M. and Frommolt, P. (2015) QuickNGS elevates next-generation sequencing data analysis to a new level of automation. *BMC Genomics*, **16**, 487.
116. Li, H. and Durbin, R. (2009) Fast and accurate short read alignment with Burrows–Wheeler transform. *Bioinformatics*, **25**, 1754–1760.
117. Feng, J.X., Liu, T., Qin, B., Zhang, Y. and Liu, X.S. (2012) Identifying ChIP-seq enrichment using MACS. *Nat. Protoc.*, **7**, 1728–1740.
118. Heinz, S., Benner, C., Spann, N., Bertolino, E., Lin, Y.C., Laslo, P., Cheng, J.X., Murre, C., Singh, H. and Glass, C.K. (2010) Simple combinations of lineage-determining transcription factors prime cis-regulatory elements required for macrophage and B cell identities. *Mol. Cell*, **38**, 576–589.
119. Kim, D., Pertea, G., Trapnell, C., Pimentel, H., Kelley, R. and Salzberg, S.L. (2013) TopHat2: accurate alignment of transcriptomes in the presence of insertions, deletions and gene fusions. *Genome Biol.*, **14**, R36.
120. Trapnell, C., Roberts, A., Goff, L., Pertea, G., Kim, D., Kelley, D.R., Pimentel, H., Salzberg, S.L., Rinn, J.L. and Pachter, L. (2012) Differential gene and transcript expression analysis of RNA-seq experiments with TopHat and Cufflinks. *Nat. Protoc.*, **7**, 562–578.
121. Trapnell, C., Williams, B.A., Pertea, G., Mortazavi, A., Kwan, G., van Baren, M.J., Salzberg, S.L., Wold, B.J. and Pachter, L. (2010) Transcript assembly and quantification by RNA-seq reveals unannotated transcripts and isoform switching during cell differentiation. *Nat. Biotechnol.*, **28**, 511–515.
122. Anders, S. and Huber, W. (2010) Differential expression analysis for sequence count data. *Genome Biol.*, **11**, R106.
123. Huang da, W., Sherman, B.T. and Lempicki, R.A. (2009) Systematic and integrative analysis of large gene lists using DAVID bioinformatics resources. *Nat. Protoc.*, **4**, 44–57.